

THE SECOND SURVEY OF THE MOLECULAR CLOUDS IN THE LARGE MAGELLANIC CLOUD BY NANTEN. I. CATALOG OF MOLECULAR CLOUDS

Y. FUKUI,¹ A. KAWAMURA,¹ T. MINAMIDANI,^{1,2} Y. MIZUNO,¹ Y. KANAI,¹ N. MIZUNO,¹ T. ONISHI,¹
Y. YONEKURA,³ A. MIZUNO,⁴ H. OGAWA,³ AND M. RUBIO⁵

Received 2006 May 24; accepted 2008 April 2

ABSTRACT

The second survey of the molecular clouds in the Large Magellanic Cloud in ^{12}CO ($J = 1-0$) was carried out by NANTEN. The sensitivity of this survey is twice as high as that of the previous NANTEN survey, leading to a detection of molecular clouds with $M_{\text{CO}} \gtrsim 2 \times 10^4 M_{\odot}$. We identified 272 molecular clouds, 230 of which are detected at three or more observed positions. We derived the physical properties, such as size, line width, and virial mass, of the 164 GMCs that have an extent more than the beam size of NANTEN in both the major and minor axes. The CO luminosity and virial mass of the clouds show a good correlation of $M_{\text{vir}} \propto L_{\text{CO}}^{1.1 \pm 0.1}$, with a Spearman rank correlation of 0.8, suggesting that the clouds are in nearly virial equilibrium. Assuming the clouds are in virial equilibrium, we derived an X_{CO} -factor of $\sim 7 \times 10^{20} \text{ cm}^{-2} (\text{K km s}^{-1})^{-1}$. The mass spectrum of the clouds is fitted well by a power law of $N_{\text{cloud}}(>M_{\text{CO}}) \propto M_{\text{CO}}^{-0.75 \pm 0.06}$ above the completeness limit of $5 \times 10^4 M_{\odot}$. The slope of the mass spectrum becomes steeper if we fit only the massive clouds, e.g., $N_{\text{cloud}}(>M_{\text{CO}}) \propto M_{\text{CO}}^{-1.2 \pm 0.2}$ for $M_{\text{CO}} \geq 3 \times 10^5 M_{\odot}$.

Subject headings: galaxies: ISM — ISM: molecules — ISM: structure — Magellanic Clouds —
radio lines: ISM — stars: formation

Online material: color figures, machine-readable tables

1. INTRODUCTION

Star formation requires a cool and high-density interstellar medium (ISM) in which most of the hydrogen is in molecular form; therefore, studies of distribution and properties of molecular clouds are very important for understanding the star formation process. Emission from the tracer CO molecule has been widely used to estimate the distribution and amount of H_2 in the Galaxy and other galaxies. Nevertheless, the CO lines in dwarf irregular galaxies are relatively weak (e.g., Ohta et al. 1993), making the surveys of molecular clouds toward dwarf galaxies difficult.

The Large Magellanic Cloud (LMC) is one of the nearest galaxies to our own. Owing to its unrivaled closeness to the solar system ($D \sim 50$ kpc) and its favorable viewing angle, studies of this galaxy have provided valuable information for our understanding of various aspects of the universe and galaxies, including the evolution of stars and stellar clusters. The LMC also provides a unique opportunity for studying molecular clouds and star formation in galaxies whose environment is different from that in the Galaxy. In the LMC, the gas-to-dust ratio is ~ 4 times higher (Koornneef 1982), and the metal abundance is about $\sim 3-4$ times lower (Rolleston et al. 2002; Dufour 1984) than that of the Galaxy.

For these reasons, the LMC has been surveyed at a wide variety of wavelengths. H I maps of moderate ($\sim 15'$) to high ($\sim 1'$) angular resolution have been obtained with the Parkes 64 m telescope (McGee & Milton 1966; Rohlfs et al. 1984; Luks & Rohlfs 1992) and with the Australian Telescope Compact Array (e.g.,

Kim et al. 1998), respectively. These studies have shown that the H I distribution is dominated by many features, such as filaments, shells, and holes. The ionized-gas content has been investigated with the aid of H α photographs (e.g., Henize 1956; Davies et al. 1976; Meaburn 1980; Kennicutt & Hodge 1986) and the radio continuum (e.g., Haynes et al. 1991; Filipovic et al. 1996; Dickel et al. 2005). The H α and radio continuum images show a variety of interstellar shells, ranging from small supernova remnants to large supergiant shells more than a few hundred parsecs across. The stellar contents of the LMC have been widely studied by photometry of the stars from the near-infrared to the optical bands (e.g., Ita et al. 2004; Zaritsky et al. 2004; Blum et al. 2006; Kato et al. 2007). In particular, the stellar clusters and associations in the LMC have been surveyed and cataloged by many authors (e.g., Lucke & Hodge 1970; Hodge 1988). Bica et al. (1996) estimated the ages of 504 stellar clusters and 120 associations based on their color indices in the UBV bands. Soft X-ray images of the LMC have also been obtained by *Röntgensatellit* (ROSAT) (Snowden & Petre 1994), revealing a variety of discrete sources, like supernova remnants, X-ray binaries, supersoft sources, and also diffuse sources associated with superbubbles and supergiant shells. Recent *Spitzer* observations cover $\sim 7^\circ \times 7^\circ$ of the LMC, revealing the distribution and properties of the dust, young stellar objects, and evolved stars (Meixner et al. 2006).

Studies of molecular gas in the LMC began with observations with either low angular resolution or a small spatial coverage. Cohen et al. (1988) obtained the first complete CO map of the LMC with the southern Center for Astrophysics 1.2 m telescope at Cerro Tololo Interamerican Observatory. However, the survey was limited by the low spatial resolution, $8.8'$, corresponding to 130 pc at the distance of the LMC. High-resolution CO observations of selected regions by the Swedish-ESO Submillimetre Telescope (SEST) 15 m telescope have been performed in the LMC (e.g., Israel et al. 1986, 2003; Johansson et al. 1994, 1998; Caldwell & Kutner 1996; Kutner et al. 1997). They have mapped some of the well-known H II regions, for example, 30 Doradus, N11, and the molecular cloud complex extending some 2 kpc south

¹ Department of Astrophysics, Nagoya University, Furocho, Chikusaku, Nagoya 464-8602, Japan.

² Department of Physics, Faculty of Science, Hokkaido University, N10W8, Kita-ku, Sapporo 060-0810, Japan.

³ Department of Physical Science, Graduate School of Science, Osaka Prefecture University, 1-1 Gakuen-cho, Nakaku, Sakai, Osaka 599-8531, Japan.

⁴ Solar-Terrestrial Environment Laboratory, Nagoya University, Furocho, Chikusaku, Nagoya 464-8601, Japan.

⁵ Departamento de Astronomía, Universidad de Chile, Casilla 36-D, Santiago, Chile.

of 30 Doradus. Although these observations revealed detailed structure of the individual molecular clouds at a linear resolution of less than 10 pc, they are limited in spatial coverage, about 1 deg^2 .

Fukui et al. (1999) carried out and completed a survey of the LMC in $\text{CO } J = 1-0$ with NANTEN, a 4 m radio telescope installed at the Las Campanas Observatory, Chile, to reveal a molecular gas distribution with resolution high enough to identify individual molecular clouds in the LMC. The 3σ noise level of the velocity-integrated intensity was $\sim 1.8 \text{ K km s}^{-1}$. This corresponds to $N(\text{H}_2) \sim 1.3 \times 10^{21} \text{ cm}^{-2}$, by using a conversion factor of $X_{\text{CO}} = 7 \times 10^{20} \text{ cm}^{-2} (\text{K km s}^{-1})^{-1}$ (see § 4.2). The first results were presented in Fukui et al. (1999) with particular emphasis on the formation of populous clusters. The catalog of 107 molecular clouds and a comparison of these molecular clouds with the H I distribution was described by Mizuno et al. (2001b). A comparison with the young stellar clusters and H II regions was the subject of Yamaguchi et al. (2001c). The comparisons of the molecular clouds with H I gas and infrared emission by the *Infrared Astronomical Satellite (IRAS)* were made by Sakon et al. (2006) and Hibi et al. (2006).

In order to have a more comprehensive understanding of the distribution and properties of the molecular clouds in the LMC, a survey in $\text{CO } J = 1-0$ with a sensitivity higher than that of the first survey has been carried out since 1999. Preliminary results focussing on the mass spectrum of this survey are presented by Fukui et al. (2001) and on the comparison of the molecular clouds with supergiant shells by Yamaguchi et al. (2001a, 2001b). Hughes et al. (2006) made a comparison of radio, far-infrared (FIR), H I , and CO in the LMC and revealed the correlation of the radio and FIR distributions.

In this paper, we present a catalog and properties of the molecular clouds from the complete data set of the second survey. Comparisons of the molecular clouds with the indication of the formation of clusters and massive stars detected in optical or radio are found elsewhere (Fukui 2005; Kawamura et al. 2007, 2008, hereafter Paper II). Fukui (2007) introduces a comparison of the molecular clouds with the H I gas distribution. Detailed studies of the H I and molecular gas distribution seeking molecular cloud formation will be presented in Y. Fukui et al. (2008, in preparation, hereafter Paper III). In this paper, the survey by NANTEN is described in § 2, and the spatial distribution and a catalog of molecular clouds are presented in § 3. We also discuss the correlations among cloud properties, such as L_{CO} , the virial mass of the molecular clouds, and the mass spectrum in § 3. A comparison of the cloud properties from the first survey and the discussion of the CO to $N(\text{H}_2)$ conversion factor are presented in § 4. Section 5 summarizes the paper.

2. OBSERVATIONS

We carried out sensitive $\text{CO } (J = 1-0)$ observations toward the LMC with NANTEN, a 4 m radio telescope of Nagoya University at Las Campanas Observatory, Chile. The half-power beamwidth was $2.6'$ at 115 GHz. The telescope had a 4 K, cooled Nb superconductor-insulator-superconductor mixer receiver, which provided a system noise temperature of $\sim 170-270 \text{ K}$, including the atmosphere toward the zenith.

The spectrometers were two acousto-optical spectrometers (AOSs) with 2048 channels; one had a velocity coverage and a resolution of 100 and 0.1 km s^{-1} , respectively. The other had a velocity coverage and a resolution of 650 and 0.65 km s^{-1} , respectively. The pointing accuracy was better than $20''$, as checked by optical observations of stars with a CCD camera attached to the telescope, as well as by radio observations of Jupiter, Venus, and the edge of the Sun. Further details about the telescope and related

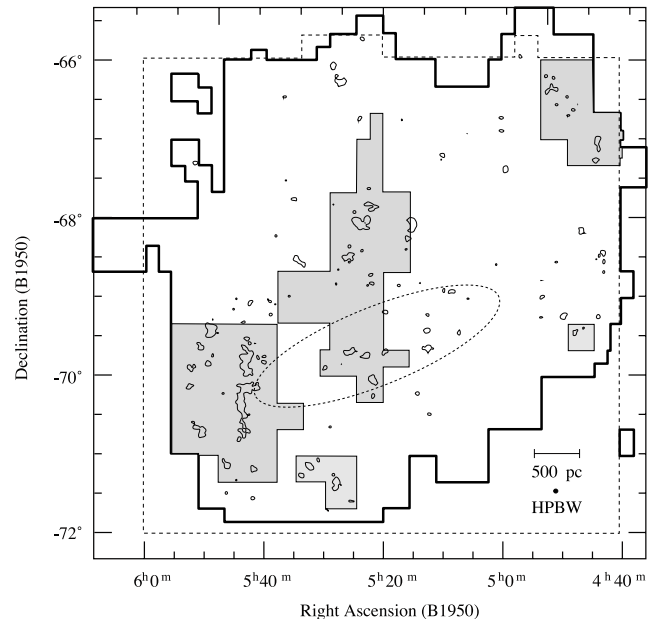


FIG. 1.—Area of survey. The boundary of the observed region in this work is indicated by the thick solid lines; the areas shaded in gray indicate the regions observed by the narrowband spectrometer (see § 2). Overlaid is the velocity-integrated intensity distribution of CO of the first survey, whose boundary is shown by the dashed line (Fukui et al. 1999; Mizuno et al. 2001b). The contours are at the 5σ noise level (3 K km s^{-1}) of the velocity-integrated intensity of the first survey, showing that the present survey covers the entire region where CO emission was detected. The ellipse illustrates the position of the bar.

instruments are given by Ogawa et al. (1990) and by Fukui & Sakakibara (1992). The spectral intensities were calibrated by employing the standard room-temperature chopper-wheel technique (Kutner & Ulich 1981). An absolute intensity calibration was made by observing Orion-KL [R.A.(B1950.0) = $5^{\text{h}}32^{\text{m}}47.0^{\text{s}}$, decl.(B1950.0) = $-5^{\circ}24'21''$] by assuming its absolute temperature T_R^* to be 65 K. We also observed the strongest peak position of the LMC, N159 [R.A.(B1950.0) = $5^{\text{h}}40^{\text{m}}1.5^{\text{s}}$, decl.(B1950.0) = $-69^{\circ}47'2''$] every 2 hr to confirm the stability of the system.

The observed region covers $\sim 30 \text{ deg}^2$ where the molecular clouds were detected by the first survey. Figure 1 shows the observed region from 1998 April to 2003 August, superposed on the integrated-intensity map of the CO from the first survey (Fukui et al. 1999; Mizuno et al. 2001b). In total, about 26,900 positions were observed in equatorial coordinates (B1950.0) in position switching. The observed grid spacing was $2'$ (corresponding to $\sim 30 \text{ pc}$ at a distance of the LMC, 50 kpc) with a $2.6'$ beam ($\sim 40 \text{ pc}$). Out of the $\sim 26,900$ positions, 6229 were observed with the narrowband spectrometer for ~ 100 days from 1998 April to November, while the rest were observed with the wideband spectrometer for ~ 300 days after 1999 March. In this paper, all the spectra observed by the narrowband spectrometer are smoothed to 0.65 km s^{-1} resolution for the reduction to have a uniform velocity resolution throughout the map. The rms noise fluctuations were $\sim 0.07 \text{ K}$ at a velocity resolution of 0.65 km s^{-1} with ~ 3 minutes integration for an on position. The typical 3σ noise level of the velocity-integrated intensity was $\sim 1.2 \text{ K km s}^{-1}$. This corresponds to $N(\text{H}_2) \sim 8 \times 10^{20} \text{ cm}^{-2}$, by using a conversion factor of $X_{\text{CO}} = 7 \times 10^{20} \text{ cm}^{-2} (\text{K km s}^{-1})^{-1}$ (see § 4.2).

3. RESULTS

3.1. Overall Distribution

Out of the $\sim 26,900$ observed positions, significant ^{12}CO ($J = 1-0$) emission, with an integrated intensity greater than

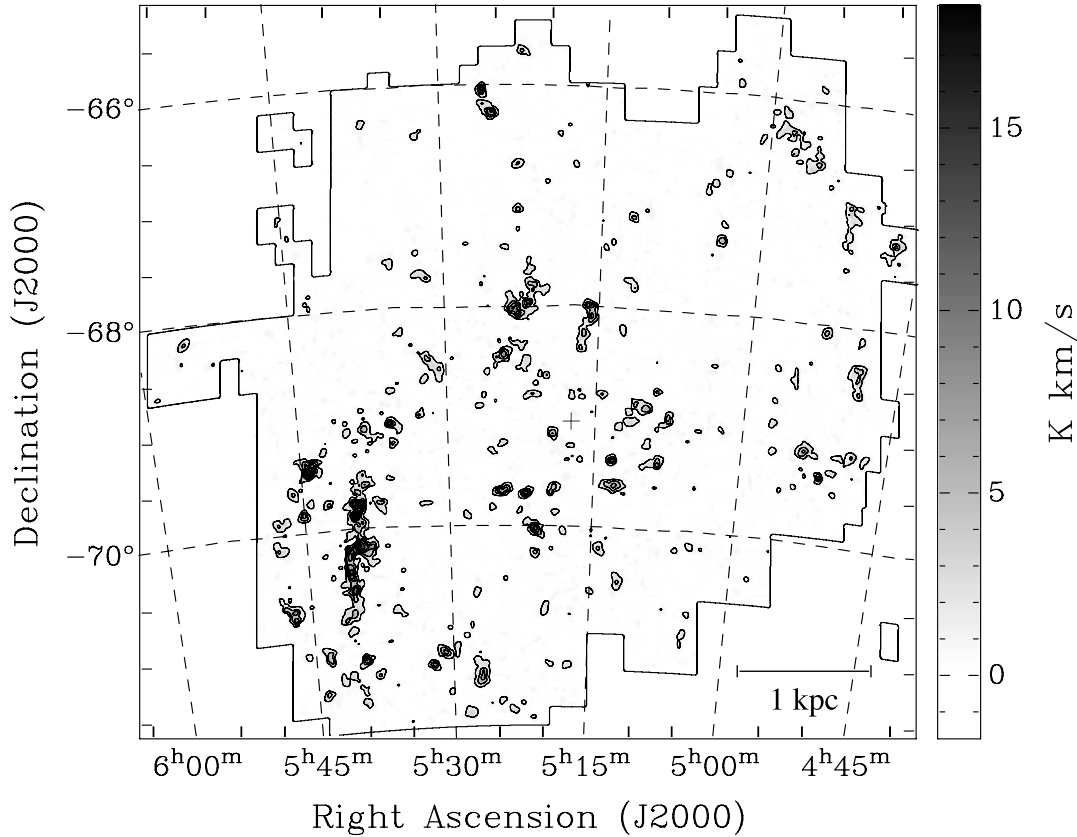


FIG. 2a

FIG. 2.—(a) Velocity-integrated map of the ^{12}CO emission integrated over $150 \leq V_{\text{LSR}} < 350 \text{ km s}^{-1}$. The contours are at 1.2 (3σ noise level), 3.6, 6.0, 8.4, 12.0, and 15.6 K km s^{-1} . The thin lines show the observed region, and the cross indicates the center determined from the kinematics of the H I observations by Kim et al. (1998). (b) Velocity-integrated map of the ^{12}CO emission superposed on an optical image. The three lowest contours from 1.2 K km s^{-1} with 2.4 K km s^{-1} intervals are shown so as not to mask the optical features. [See the electronic edition of the Supplement for a color version of this figure.]

1.2 K km s^{-1} (the $\sim 3\sigma$ noise level), was detected at about 1300 positions, which corresponds to $\sim 5\%$ of the total observed positions. The total velocity-integrated intensity distribution of the molecular gas is shown in Figure 2a.

The mass of the molecular gas in total is $\sim 5 \times 10^7 M_{\odot}$, if we use a CO luminosity to hydrogen column density conversion factor, the X_{CO} -factor, of $\sim 7 \times 10^{20} \text{ cm}^{-2} (\text{K km s}^{-1})^{-1}$ (see § 4). The CO distribution of the LMC is found to be clumpy with several large molecular cloud complexes, unlike the H I gas distribution, which is composed of many filamentary and shelllike structures (e.g., Kim et al. 1999). These clumps of the molecular gas tend to be detected toward the intensity peak of the H I gas as shown in Blitz et al. (2007), Fukui (2007), and Paper III. The cloud complex south of 30 Doradus at $\alpha(\text{J2000}) \sim 5^{\text{h}}40^{\text{m}}$ and $\delta(\text{J2000}) \sim -71^{\circ}$ to $-69^{\circ}30'$ is remarkable, stretching in a nearly straight line from north to south, as already noted by the previous CO observations (Cohen et al. 1988; Fukui et al. 1999; Mizuno et al. 2001b). The current survey shows that the clouds in this molecular cloud complex, “the molecular ridge” are actually connected to one another by a low-density molecular gas, while the first survey traced only the densest regions and identified the molecular ridge as consisting of two or three discrete entities. The arclike distribution of molecular clouds along the southeastern optical edge of the galaxy (the “CO Arc” in Fukui et al. 1999 and Fukui 2002) is also clearly seen. The current sensitive survey confirms that this CO Arc indeed clearly represents an arclike edge of the molecular gas distribution in this eastern boundary of the LMC.

Other CO clouds are distributed over the observed area with moderate concentration toward several prominent H II regions

[e.g., N 44 at $\alpha(\text{J2000.0}) \sim 5^{\text{h}}22^{\text{m}}$ and $\delta(\text{J2000.0}) \sim -68^{\circ}$, N11 at $\alpha(\text{J2000.0}) \sim 4^{\text{h}}55^{\text{m}}$ and $\delta(\text{J2000.0}) \sim -66^{\circ}30'$] and the “bar” (e.g., clouds around $\alpha \sim 5^{\text{h}}20^{\text{m}}$ and $\delta \sim -70^{\circ}$). The small molecular clouds are more clearly observable in the current survey, especially, toward a supergiant shell, LMC 4, at $\alpha(\text{J2000.0}) \sim 5^{\text{h}}20^{\text{m}}\text{--}5^{\text{h}}40^{\text{m}}$ and $\delta(\text{J2000.0}) \sim -68^{\circ}$ to -66° (see also Yamaguchi et al. 2001a). A detailed comparison of the molecular gas with the indicators of star formation, such as H α or radio continuum, will be discussed elsewhere (Paper II).

Figure 3 is a histogram of the integrated intensity, I.I., of each observed position with I.I. $> 0.4 \text{ K km s}^{-1}$ ($\sim 1\sigma$ noise level). About 980 observed positions have $N(\text{H}_2) > 10^{21} \text{ cm}^{-2}$, while only four positions have $N(\text{H}_2) > 10^{22} \text{ cm}^{-2}$.

Figure 4a shows the radial distribution of CO emission; the surface density, Σ , is derived by integrating the CO luminosity within annuli spaced by $4'$ and then dividing by the area of the annuli. The center used is $\alpha(\text{J2000.0}) = 5^{\text{h}}17.6^{\text{m}}$, $\delta(\text{J2000.0}) = -69^{\circ}2'$, which was determined from the kinematics of the H I observations by Kim et al. (1998). To see the angular distribution of the CO emission, the distribution of the surface density, Σ , derived by integrating the CO luminosity over a sector with a 10° width and then dividing by an observed area of the sector is shown in Figure 4b. The CO luminosity to mass conversion is carried out by assuming a conversion factor, X_{CO} , of $7 \times 10^{20} \text{ cm}^{-2} (\text{K km s}^{-1})^{-1}$ (see § 4.2) for both.

Figure 4 indicates that the radial profile of the molecular gas decreases moderately along the galactocentric distance, as is also seen in nearby spiral galaxies (e.g., Wong & Blitz 2002), although the profile does not really fit to a power law as they do for the spiral

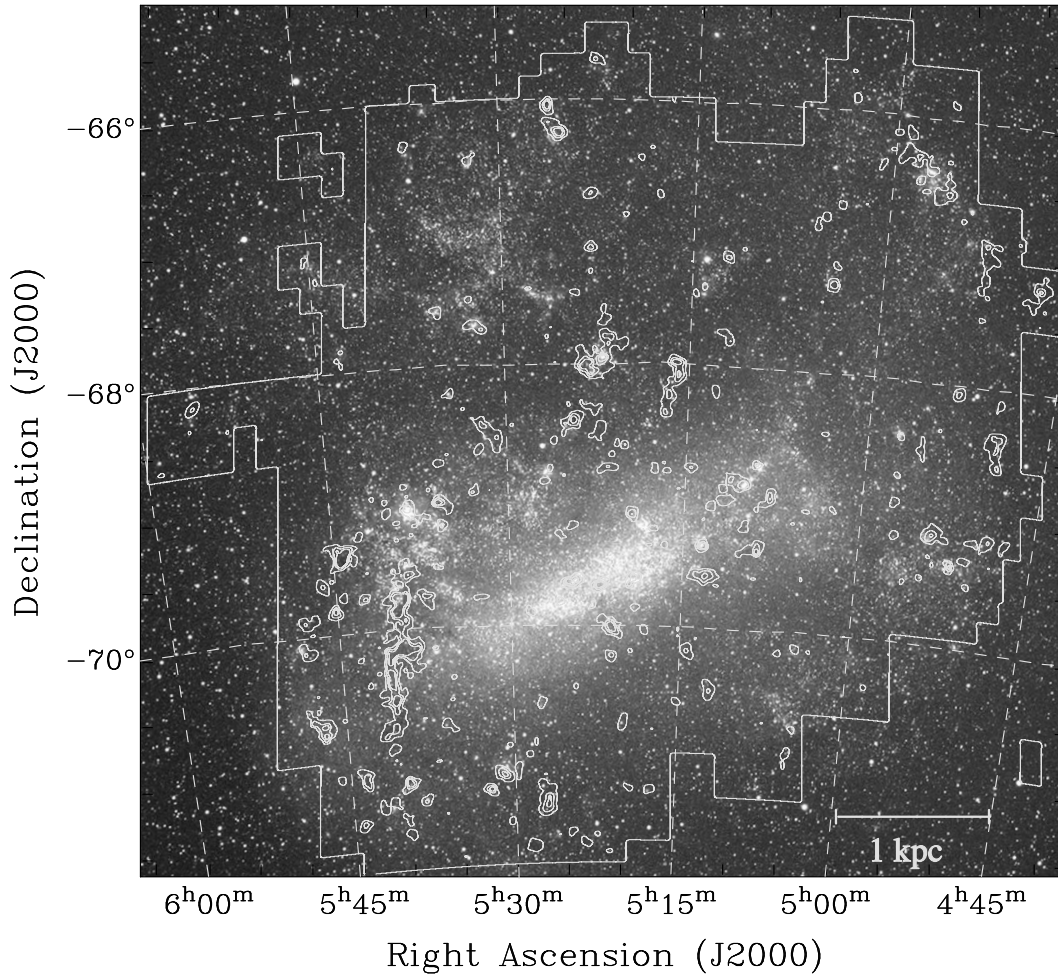


FIG. 2b

galaxies (Wong & Blitz 2000). It is interesting to note the sharp enhancement of the surface density around 2 kpc. This enhancement is due to the molecular cloud complexes, the molecular ridge, N11, and N44. This enhancement is also seen in the angular distribution, especially at about 120° due to the molecular ridge. Compared with the nearby galaxies of Wong & Blitz (2002), the local enhancement of the molecular gas is more conspicuous in the LMC.

Figures 5a–5l are a series of channel maps that show the velocity distribution; they present channel maps with velocities at (a) 200–210, (b) 210–220, (c) 220–230, (d) 230–240, (e) 240–250, (f) 250–260, (g) 260–270, (h) 270–280, (i) 280–290, (j) 290–300, (k) 300–310, and (l) 310–320 km s^{-1} .

In the velocity range 200–240 km s^{-1} , the CO Arc in the southeastern boundary of the LMC and the molecular ridge from the south of 30 Doradus are prominent. The two molecular cloud complexes associated with active star-forming regions N11 and N44 are also prominent in the velocity range between 270–290 km s^{-1} . A systematic velocity gradient from the southeast to the northwest has been known from the first survey (Mizuno et al. 2001b). Our sensitive survey shows a clear feature in the northeast at high velocities, corresponding to LMC 4, in addition to the overall velocity gradient already observed in the first survey. Detailed comparisons of the velocity and spatial distributions of the H I and CO emission will be presented in Paper III.

3.2. Identification of CO Molecular Clouds

To study the properties of the molecular gas in the LMC, individual cloud was identified by the cloud-finding algorithm,

FITSTOPROPS (Rosolowsky & Leroy 2006). First, the intensity data cube is converted to a signal-to-noise-ratio (S/N) data cube by dividing through by the noise at each position to search for significant emission by clipping the maps at a constant S/N; a constant S/N is used instead of a constant flux-density threshold, although the sensitivity variation across the map is not large (Fig. 6). Then, pairs of adjacent velocity channels with normalized flux greater than 3 were searched for. For each pair, these velocity channels and all contiguous data pixels with normalized flux greater than 2 were assigned to a candidate molecular cloud. This process was continued until all the pairs of adjacent channels with normalized flux greater than 3 have been identified as candidate clouds.

We identified 272 clouds, of which 230 were detected at more than two observed positions. In this paper, we shall call these 230 clouds with more than two observed positions “the giant molecular clouds [GMCs].” The position and intensity-weighted mean velocity of the 230 GMCs and the rest (“the small clouds,” in the following) are listed in Tables 1 and 2, respectively.

The sensitivity of a data set influences the cloud properties derived from that data as emphasized by Rosolowsky & Leroy (2006). In order to reduce the observational bias and to be able to compare data sets with different S/N levels, the boundary of a cloud is extrapolated to a boundary isosurface of $T_{\text{edge}} = 0$ K (see also Blitz & Thaddeus 1980; Scoville et al. 1987). The major and minor axes, size R , position angle (P.A.), and virial mass M_{vir} are derived for 164 GMCs (hereafter Group A GMCs) out of 230; the rest (hereafter Group B) have a minor axis less than the

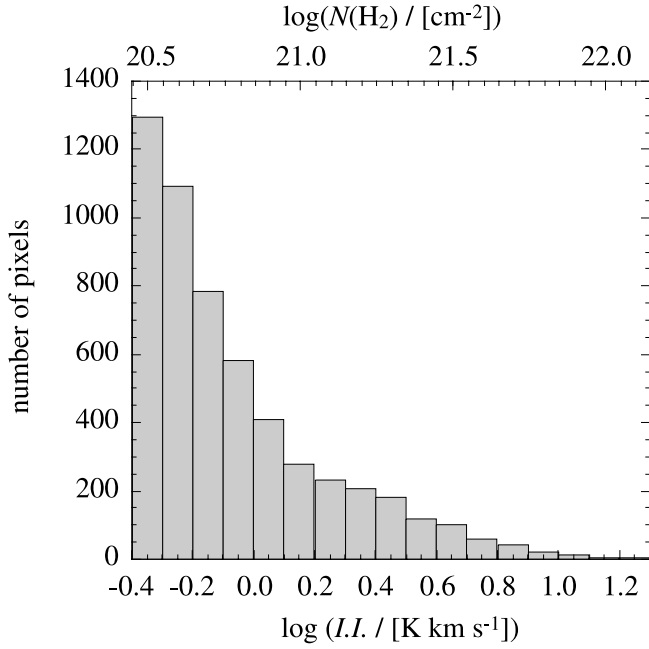


FIG. 3.—Distribution of the integrated intensities greater than 0.4 K km s^{-1} ($\sim 1 \sigma$ noise level). The equivalent values of the column density derived from the integrated intensity by using $X_{\text{CO}} = 7 \times 10^{20} \text{ cm}^{-2} (\text{K km s}^{-1})^{-1}$ are also shown.

NANTEN beam, so that the size is not derivable by using the deconvolved moment. The line width, ΔV , and the CO luminosity, L_{CO} , are less sensitive to the beam dilution than the cloud size, so that we can determine ΔV and L_{CO} of both the Group A and B GMCs. Then, M_{CO} , the molecular cloud mass, is derived from L_{CO} by using $X_{\text{CO}} = 7 \times 10^{20} \text{ cm}^{-2} (\text{K km s}^{-1})^{-1}$, as derived in § 4.2 by assuming virial equilibrium and the mass fraction of helium to be 36%. The procedure to derive these properties is described by Rosolowsky & Leroy (2006) in detail. The derived properties are presented in Table 3.

3.3. Properties of the Molecular Clouds

In this section, we consider the Group A GMCs, which are resolved by NANTEN. The Group A GMCs have radii ranging from 10 to 220 pc, line widths between 1.6 and 20.2 km s^{-1} , CO luminosities between 1.4×10^3 and $7.1 \times 10^5 \text{ K km s}^{-1} \text{ pc}^2$, and virial masses ranging from 9×10^3 to $9 \times 10^6 M_{\odot}$.

Figure 7 shows the frequency distribution of the V_{LSR} of the clouds. The distribution is rather nonuniform having peaks at ~ 220 – 250 and ~ 280 – 290 km s^{-1} . The one at $V_{\text{LSR}} \sim 220$ – 250 km s^{-1} represents the clouds in the southern part of the LMC, including the molecular ridge and the CO Arc as seen in Figures 5c–5e. The other at $V_{\text{LSR}} \sim 280$ – 290 km s^{-1} is dominated by the emission from the LMC 4, N44, and N11 regions (Figs. 5i–5j).

Figures 8 and 9 are the histograms of the ratio of the major and minor axes and the P.A. of the GMCs, respectively. The frequency distribution of P.A. is rather uniform. The distribution of the ratio of the major and minor axes has a peak at ~ 1.7 , with an average of 2.5, indicating that clouds are generally elongated.

In order to see if the cloud has an alignment with the large-scale structure of the galaxy, such as a spiral pattern, here we introduce a parameter, θ , the angle between the major axis and the tangent at the molecular cloud of a circle with a radius, d_{cen} (Fig. 10a). Figure 10b shows the frequency distribution of θ . Since the uncertainties of the P.A., as well as of θ , depend on the ratio of the major and minor axes, the histogram of θ is divided

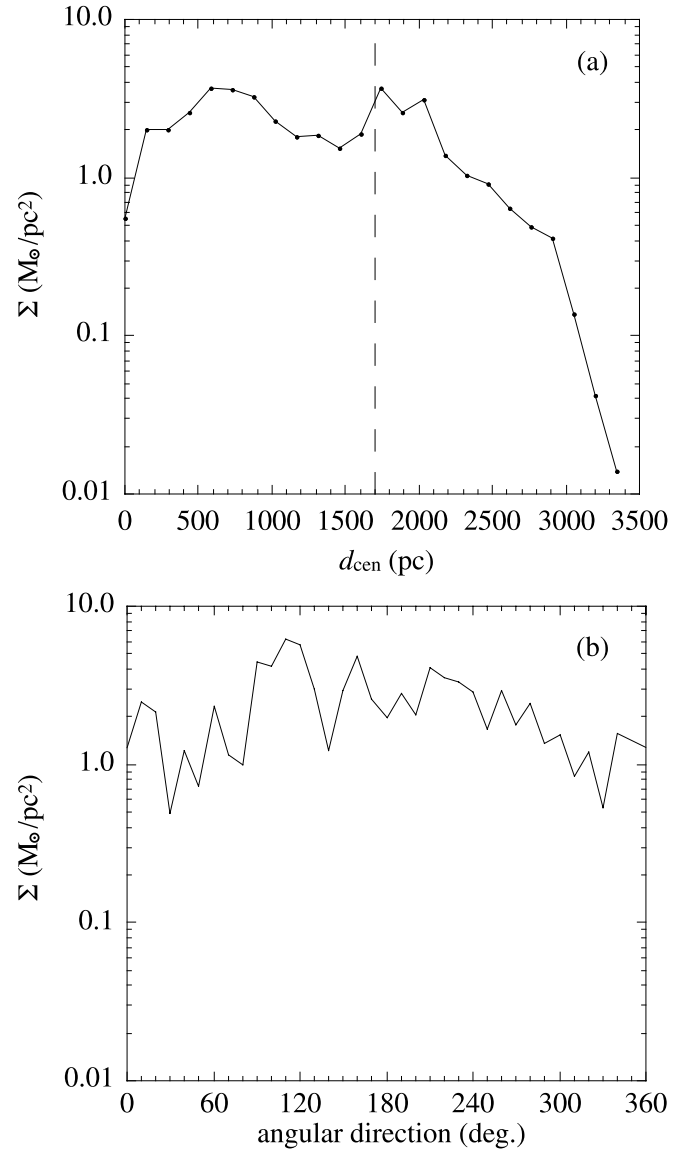


FIG. 4.—(a) Distribution of the surface density along the distance from the center $\alpha(\text{J2000.0}) = 5^{\text{h}}17.6^{\text{m}}$, $\delta(\text{J2000.0}) = -69^{\circ}2'$ determined from the kinematics of the H I (Kim et al. 1998). The region within 1.7 kpc from the center (*dashed line*) is completely covered by the current survey. The surface density is derived by dividing the mass of the clouds by the area covered by the survey. (b) Distribution of the surface density along the P.A. starting from north to east in a counterclockwise direction with respect to the kinematic center in (a).

into three groups according to the axial ratio. The histogram of θ shows the number distribution is nearly uniform and does not have any particularly favorable angles. To see if the distribution of θ has any characteristics with the galactocentric distance, Figure 10c shows a plot of d_{cen} versus θ . Again, the plots are distributed quite uniformly, showing no strong dependence of θ on d_{cen} .

3.3.1. Line Width–Size relation

In this section, we present the correlation between the line width and the radius of the GMCs. The size, R , of the cloud is computed as a geometric mean of the “deconvolved” second spatial moments along the major and minor axes, which were derived by using principal component analysis: we “deconvolve” the beam by subtracting its size from the measured cloud size in quadrature. A FWHM line width, ΔV , is derived by multiplying

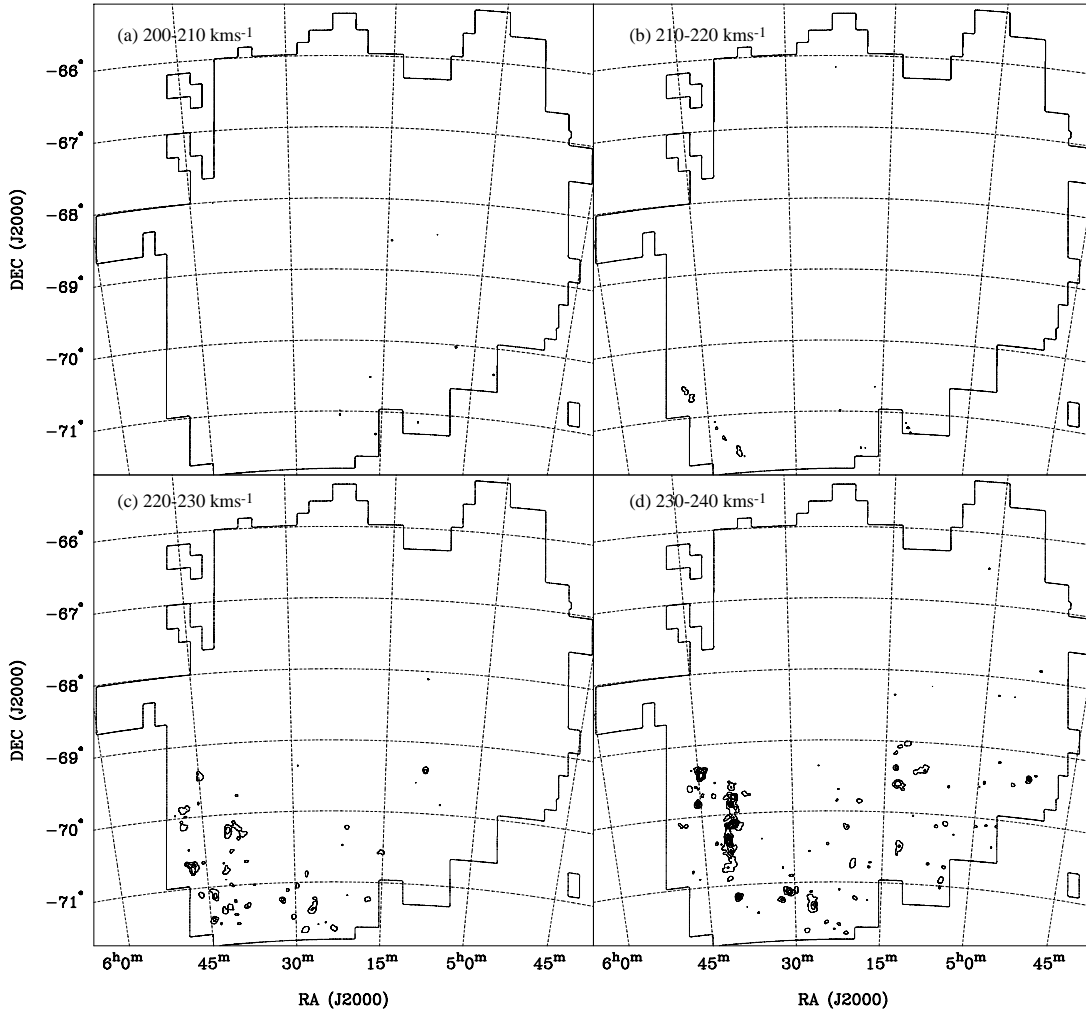


FIG. 5.—Velocity-integrated maps of the ^{12}CO emission integrated over (a) $200 \leq V_{\text{LSR}} < 210$, (b) $210 \leq V_{\text{LSR}} < 220$, (c) $220 \leq V_{\text{LSR}} < 230$, (d) $230 \leq V_{\text{LSR}} < 240$, (e) $240 \leq V_{\text{LSR}} < 250$, (f) $250 \leq V_{\text{LSR}} < 260$, (g) $260 \leq V_{\text{LSR}} < 270$, (h) $270 \leq V_{\text{LSR}} < 280$, (i) $280 \leq V_{\text{LSR}} < 290$, (j) $290 \leq V_{\text{LSR}} < 300$, (k) $300 \leq V_{\text{LSR}} < 310$, and (l) $310 \leq V_{\text{LSR}} < 320 \text{ km s}^{-1}$. The contours are from 1 K km s^{-1} with 1 K km s^{-1} intervals. The thin lines indicate the observed region.

the moment of the velocity within a GMC by $[8 \ln(2)]^{1/2}$ (see also Rosolowsky & Leroy 2006). Figure 11 shows a plot of $\log(\Delta V)$ versus $\log(R)$ of the Group A GMCs. It has been known that the line width and the size of molecular clouds have a good correlation of $\sigma_v \propto R^{0.5}$ in the solar vicinity (Larson 1981) and in the inner Galaxy (e.g., Dame et al. 1986; Solomon et al. 1987), while the correlation in the GMCs in this work is rather weak, and the best-fitting power law is $\Delta V = 1.3R^{0.2}$, with a Spearman rank coefficient of 0.3. It is likely that the lack of the dynamic range in size may make the correlation lower in the present study than for the Galactic clouds, although we see a weak positive correlation in the LMC GMCs.

We have applied the cloud-identifying algorithm of Rosolowsky & Leroy (2006) with the parameters used in the current study to identify the GMCs in the LMC to the molecular clouds in the Small Magellanic Cloud (SMC; Mizuno et al. 2001a) as well as those in the outer Galaxy, the Warp region (Nakagawa et al. 2005), and derived the physical properties. When we add the clouds in the SMC and the Warp region to the plot of Figure 11a, the dynamic range in R becomes larger, and a positive correlation is seen. A line width–size relation $\sigma_v \propto R^{0.5}$ seen in the inner Galaxy by Solomon et al. (1987) is also shown as an example in Figure 11 (thin dotted line). The correlation between the line width and size of the clouds in the LMC, the SMC, and the Warp region does seem to be consistent with a power-law relation $\sigma_v \propto R^{0.5}$ but

with a clear offset from the relation determined for the inner Galaxy (Solomon et al. 1987). Note that at least a part of this offset can be attributed to differences in the methods used to measure cloud properties. The sense of the offset is that for a given radius, the clouds in the inner Galaxy have larger line widths. This may be partially due to the relatively high value of T_A used by Solomon et al. (1987) to define the cloud radius, implying that the clouds might be smaller for a given value of ΔV .

3.3.2. Virial Mass–CO Luminosity Relation

The determination of the mass of molecular hydrogen gas is fundamental for understanding the physics of the ISM and star formation in galaxies. In this subsection, we compare the virial mass and the CO luminosity and discuss the conversion factor from the CO line intensity to the H_2 column density in the LMC.

Figure 12 shows the virial mass, M_{vir} , as a function of luminosity, L_{CO} , of the clouds in the LMC (filled circles). The plot shows a tight power law for the mass–luminosity relation with some dispersion. A least-squares fit to the data gives a power law, $[M_{\text{vir}}/M_{\odot}] = 26[L_{\text{CO}}/(\text{K km s}^{-1} \text{ pc}^2)]^{1.1 \pm 0.3}$, with a Spearman rank correlation of 0.8. This relation suggests that clouds are virialized and the CO luminosity can be a good tracer of mass in the LMC with a quite-constant conversion factor from L_{CO} to mass throughout the mass range $10^4 \lesssim M_{\text{vir}}/M_{\odot} \lesssim 10^7$. We have added the reidentified clouds in the SMC (Mizuno et al. 2001a)

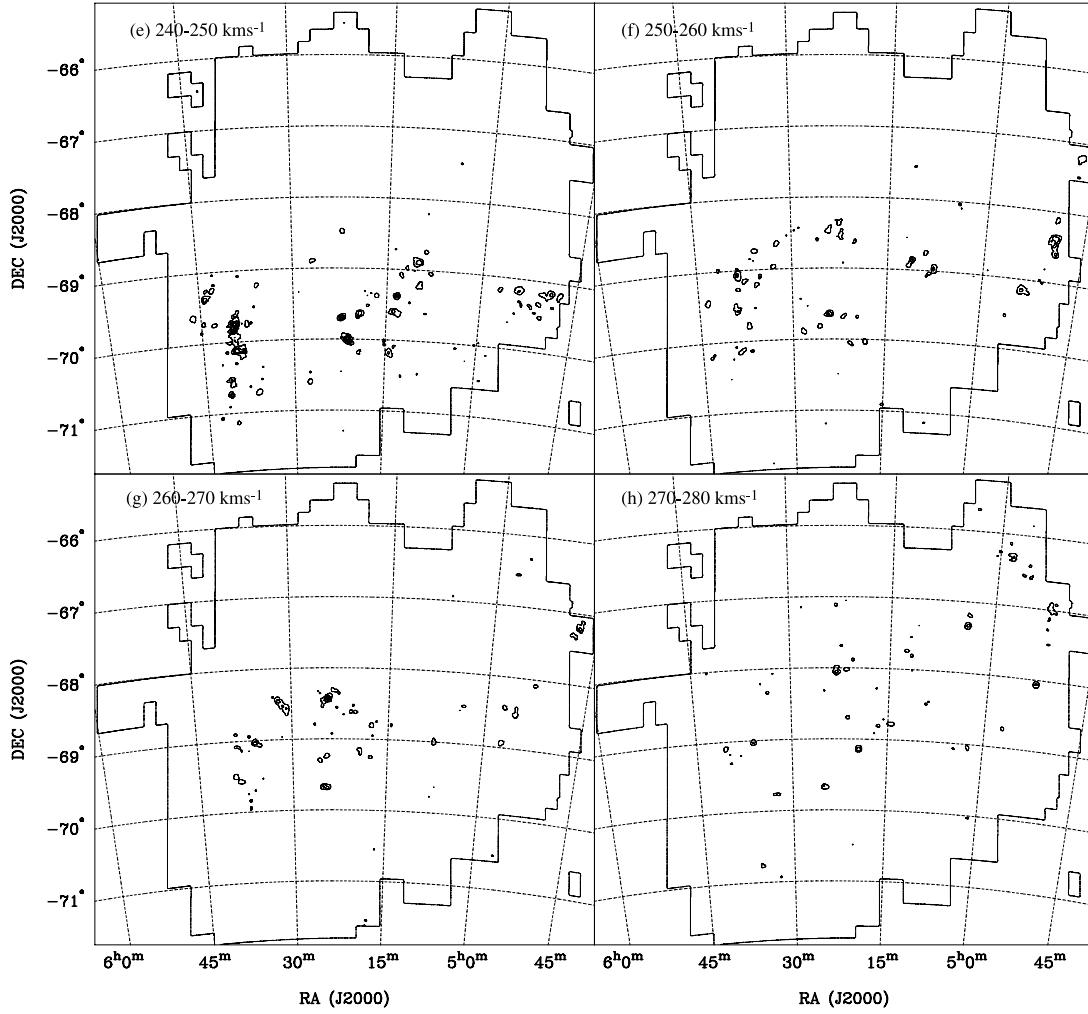


FIG. 5—Continued

and the Warp region (Nakagawa et al. 2005) to Figure 12 as in § 3.3.1. The clouds in the SMC and the Warp region lie along the best-fitting power law of GMCs in the LMC.

3.3.3. Mass Spectrum

The frequency distribution of the cloud masses has an important impact not only on the star formation but also on cloud formation and destruction. The mass spectrum of the clouds is well fitted by a power law and often presented as $dN/dM \propto M^{-(\alpha+1)}$, or $N_{\text{cloud}}(>M) \propto M^{-\alpha}$. The preliminary results of the mass spectrum by the second NANTEN survey in the LMC have been already presented and discussed in Fukui et al. (2001). They found the mass spectrum derived from the CO luminosity has a slope with $\alpha = 0.9 \pm 0.1$ above the completeness limit of $8 \times 10^4 M_{\odot}$.

In this section, we present the spectra of the masses, M_{CO} , derived from the CO luminosity, L_{CO} , and a conversion factor, $X_{\text{CO}} = 7 \times 10^{20} \text{ cm}^{-2} \text{ K km s}^{-1}$ (§ 3.2 and § 4.2). Here, the CO luminosity, L_{CO} , is less sensitive to the beam dilution than the cloud size, so that we can consider that not only the Group A GMCs but also the L_{CO} of the Group B GMCs, for which we could not derive a size and M_{vir} , are determined well enough to obtain M_{CO} (§ 3.2 and Table 3). The mass spectrum of M_{CO} including both the Group A and B GMCs is shown in Figure 13. The maximum likelihood method (Crawford et al. 1970) was

applied to obtain the best-fitting power law above the completeness limit, $5 \times 10^4 M_{\odot}$. The best-fitting power law above the completeness limit is $N_{\text{cloud}}(\geq M_{\text{CO}}) = 6.6 \times 10^5 M^{-0.75 \pm 0.06} - 3.4$.

The results indicate that the mass of the molecular gas in the LMC is concentrated in the massive clouds, since $\alpha < 2$. The slope of the mass spectrum, and thus the fact that the massive clouds contribute to the galactic total mass, is consistent within the current results, as well as with those presented by Fukui et al. (2001), although the current results show a shallower slope than the other. This difference in the index values of the best-fitting power law may be explained by the difference in the completeness limit. Table 4 shows the index value, α , of the power-law fit to the different mass ranges of the GMCs. The best-fitting power law obtained for the clouds with $M_{\text{CO}} \geq 3 \times 10^5 M_{\odot}$ is shown in Figure 13 as an example. Table 4 indicates that the slope of the mass spectrum becomes steeper if we fit only the massive clouds, e.g., $N_{\text{cloud}}(>M_{\text{CO}}) \propto M_{\text{CO}}^{-1.2 \pm 0.2}$ for $M_{\text{CO}} \geq 3 \times 10^5 M_{\odot}$, and the logarithmic slope of the mass spectrum becomes steeper at $\sim 3 \times 10^5 M_{\odot}$.

4. DISCUSSION

4.1. Comparison with the First Survey

The current survey was carried out to cover the regions where the molecular clouds are detected in the first survey. The S/N

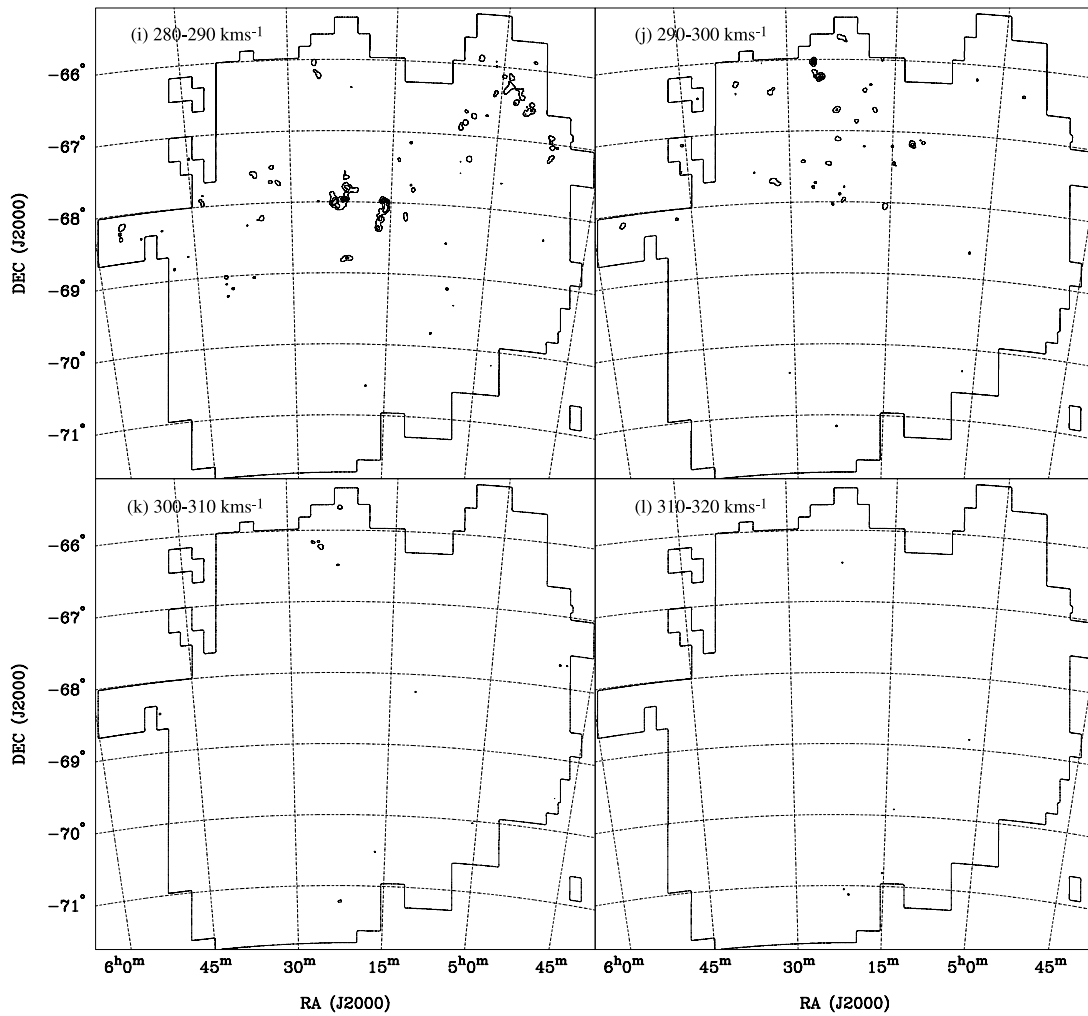


FIG. 5—Continued

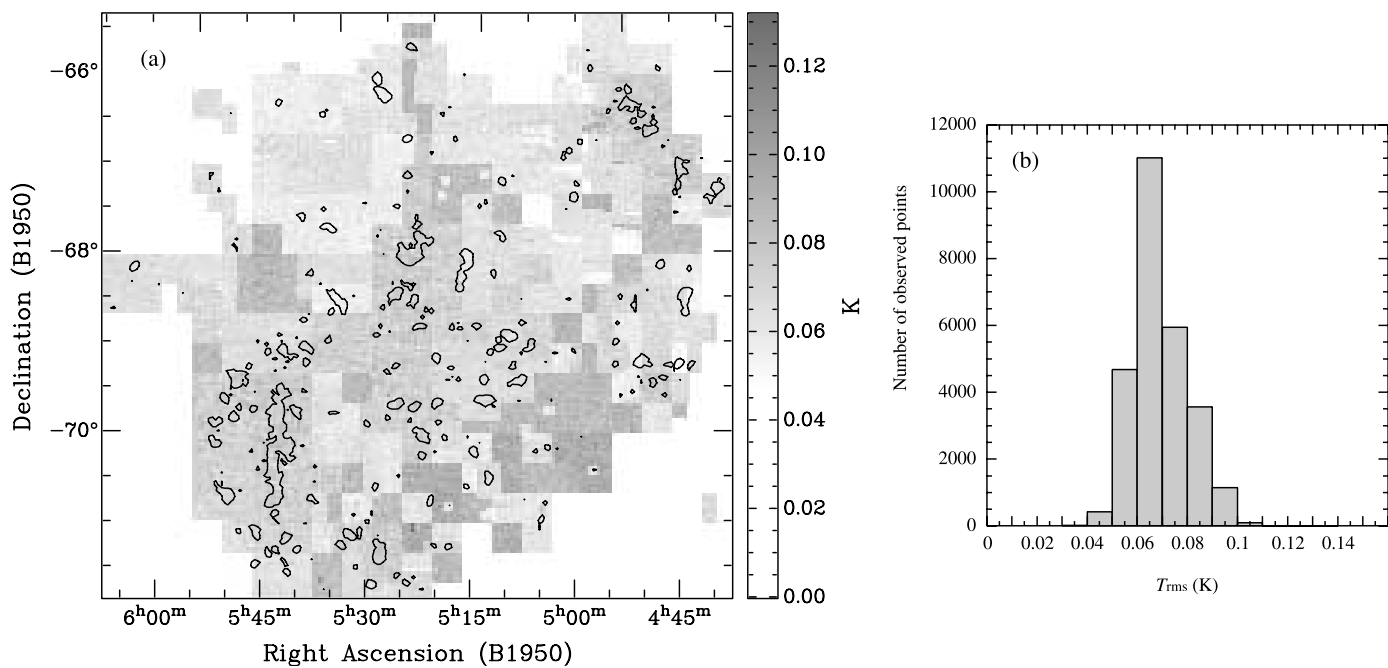


FIG. 6.—(a) Spatial distribution of the noise fluctuations per AOS channel of the current survey and (b) frequency distribution of the noise fluctuations.

TABLE 1
CATALOG OF 230 GMCs

NUMBER	NAME ^a	POSITION ^b				V_{LSR}^c (km s ⁻¹)
		$\alpha(2000.0)$	$\delta(2000.0)$	$\alpha(1950.0)$	$\delta(1950.0)$	
1.....	LMC N J0447–6910	04 47 30.4	–69 10 8.9	04 47 44.0	–69 15 20.2	239.4
2.....	LMC N J0447–6713	04 47 35.9	–67 13 44.0	04 47 33.8	–67 18 55.4	256.8
3.....	LMC N J0448–6920	04 48 40.8	–69 20 41.3	04 48 56.2	–69 25 47.6	238.9
4.....	LMC N J0449–6910	04 49 12.4	–69 10 21.0	04 49 26.4	–69 15 25.2	240.3
5.....	LMC N J0449–6826	04 49 24.2	–68 26 49.8	04 49 32.0	–68 31 53.4	249.4

NOTES.—Units of right ascension are hours, minutes, and seconds, and units of declination are degrees, arcminutes, and arcseconds. Table 1 is also available in machine-readable form in the electronic edition of the *Astrophysical Journal Supplement*.

^a Name of the clouds; “N” stands for “NANTEN.”

^b Position of the clouds derived from an intensity-weighted mean over all the pixels of a cloud.

^c LSR velocity derived from an intensity-weighted mean of the velocity distribution within a cloud.

of the present observations was higher by a factor of 2 than those in the first NANTEN survey (Fukui et al. 1999; Mizuno et al. 2001b; Yamaguchi et al. 2001c). This increase in sensitivity made it possible to increase the number of significant detections and identified clouds. Different cloud-identification criteria are used in the current study and in Fukui et al. (1999) and Mizuno et al. (2001b). Nevertheless, the number of the clouds with more than two observing positions (“the large clouds” in Mizuno et al. 2001b) is a factor of 3 larger in the present survey even if we use the same algorithm and criteria.

Here we compare the line width–size relation and the virial mass–CO luminosity relation of the molecular clouds from the first and the current surveys. To compare the results, we recalculated the size and the virial mass of the large clouds of the first survey by subtracting the NANTEN beam from the size in Table 1 of Mizuno et al. (2001b).

Figure 14 is a plot of the line width and the size of the clouds derived from both the first survey (*gray filled circles*) and the current survey (*filled circles*). The clouds from both the current and the first survey show a large scatter with little positive correlation of the line width and the size. An offset from the correlation of the inner Galaxy is also seen. The scatter is larger in the current survey. This may be explained by the difference in the sensitivity; the high sensitivity of the current survey made it possible to decompose a cloud into several individual clouds with different velocities along the same line of sight, although these clouds may have been identified as a single entity by the first survey.

Figure 15 is a plot of the virial mass, M_{vir} , as a function of luminosity, L_{CO} , of the Group A GMCs from the current survey

(*filled circles*) and the 55 clouds from the first survey (*open circles*). The correlations between the M_{vir} and L_{CO} in both surveys are consistent within the error. Again, the scatter in the current survey is larger, but because the higher sensitivity limit of the current survey enlarges the dynamic range in M_{vir} and L_{CO} , the correlation coefficient remains as high as 0.85. The ratio of M_{vir} and L_{CO} is related to the conversion factor, X_{CO} -factor, from the CO luminosity to the hydrogen column density, $N(\text{H}_2)$. The consistency of the M_{vir} and L_{CO} relation in both surveys suggests that the X_{CO} -factors derived from both surveys are also consistent.

4.2. CO to $N(\text{H}_2)$ Conversion Factor

In the following, we derive the X_{CO} -factor from the current survey. The determination of the mass of H_2 in galaxies is fundamental for an understanding of interstellar physics and star formation. The principal method for obtaining H_2 masses converts the intensity of the CO molecular line emission, I_{CO} , into the column density of H_2 molecules. The conversion factor, or X -factor [$X \equiv N(\text{H}_2)/I_{\text{CO}} = M_{\text{H}_2}/L_{\text{CO}}$], has been derived for molecular clouds in the solar vicinity based on the assumption of virial equilibrium of individual clouds (e.g., Young & Scoville 1991). This method has been also used to derive the conversion factors in nearby galaxies where individual clouds are resolved, such as the LMC, SMC, M31, M33, etc., (e.g., Mizuno et al. 2001a, 2001b; Wilson & Scoville 1990).

The plot of the M_{vir} against L_{CO} in § 3.3.2 (Fig. 12) from the current survey suggests that for massive clouds, $M_{\text{CO}} > 10^5 M_{\odot}$, it is reasonable to assume virial equilibrium. Here, we use the conventional method of applying the virial theorem to the clouds to estimate the X_{CO} -factor in the LMC. The average value of

TABLE 2
CATALOG OF 42 SMALL CLOUDS

NUMBER ^a	NAME	POSITION ^b				V_{LSR}^c (km s ⁻¹)
		$\alpha(2000.0)$	$\delta(2000.0)$	$\alpha(1950.0)$	$\delta(1950.0)$	
231.....	LMC N J0447–6728	04 47 18.3	–67 28 47.5	04 47 18.0	–67 34 0.1	250.0
232.....	LMC N J0448–6721	04 48 1.7	–67 21 53.9	04 48 0.7	–67 27 3.6	254.1
233.....	LMC N J0449–6810	04 49 40.6	–68 10 12.9	04 49 46.2	–68 15 15.5	255.2
234.....	LMC N J0451–6927	04 51 21.8	–69 27 4.8	04 51 38.8	–69 31 59.9	237.7
235.....	LMC N J0453–6846	04 53 55.9	–68 46 38.1	04 54 7.5	–68 51 22.7	242.7

NOTE.— Table 2 is also available in machine-readable form in the electronic edition of the *Astrophysical Journal Supplement*.

^a Name of the clouds; “N” stands for “NANTEN.”

^b Position of the clouds derived from an intensity-weighted mean over all the pixels of a cloud.

^c LSR velocity derived from an intensity-weighted mean of the velocity distribution within a cloud.

TABLE 3
PROPERTIES OF 230 GMCs

NUMBER	NAME	CLOUD PROPERTIES ^a						
		ΔV_{LSR} (km s^{-1})	R^b (pc)	P.A. (deg)	Maj _{nodeconv} × Min _{nodeconv} ^c (pc × pc)	L_{CO} ($10^4 \text{ K km s}^{-1} \text{ pc}^2$)	M_{vir}^b ($10^5 M_{\odot}$)	M_{CO} ($10^5 M_{\odot}$)
1.....	LMC N J0447–6910	4.2		46	32 × 15	1		2
2.....	LMC N J0447–6713	11.2	97	54	69 × 42	7	20	10
3.....	LMC N J0448–6920	4.1		169	39 × 14	0.5		0.7
4.....	LMC N J0449–6910	5.3	60	23	51 × 26	3	3	4
5.....	LMC N J0449–6826	5.7	87	87	79 × 31	8	5	10

NOTE.—Table 3 is available in its entirety in the electronic edition of the *Astrophysical Journal Supplement*. A portion is shown here for guidance regarding its form and content.

^a Observed properties of the GMCs: The FWHM of the line width, ΔV_{LSR} , is derived from multiplying $[8 \ln(2)]^{1/2}$ to a second moment of the spectra within a cloud, and the size, R , is a geometric mean of the beam-deconvolved second spatial moment along the major and minor axis, respectively. The P.A., major and minor axes without beam deconvolution, CO luminosity L_{CO} , virial mass M_{vir} , and mass M_{CO} are also listed. The mass M_{CO} is derived from L_{CO} with $X_{\text{CO}} = 7 \times 10^{20} \text{ cm}^{-2} (\text{K km s}^{-1})^{-1}$. See also § 3.2 for the derivation of the cloud properties.

^b The radius and the virial mass are indicated by quotes when the minor axis of the cloud is less than the NANTEN beam and the beam-deconvolved minor axis is not derivable.

^c A minor axis without beam deconvolution is indicated by quotes when the cloud is detected only at one observed point along the minor axis and the minor axis without deconvolution is not derivable.

$\log(M_{\text{vir}}/L_{\text{CO}})$ is 1.2 ± 0.3 , corresponding to $X_{\text{CO}} = (7 \pm 2) \times 10^{20} \text{ cm}^{-2} (\text{K km s}^{-1})^{-1}$, for the Group A GMCs with L_{CO} higher than the completeness limit, $9 \times 10^3 \text{ K km s}^{-1} \text{ pc}^2$, which is equivalent to $M_{\text{vir}} \geq 1.4 \times 10^5 M_{\odot}$. Figure 16 is a frequency distribution of $\log(M_{\text{vir}}/L_{\text{CO}})$ of the Group A GMCs, i.e., including all the clouds for which we derived virial masses. The geometric mean of $M_{\text{vir}}/L_{\text{CO}}$, and thus the X_{CO} -factor, does not differ from the values obtained by using the clouds with $L_{\text{CO}} \geq 9 \times 10^3 \text{ K km s}^{-1} \text{ pc}^2$ only. This value is slightly less than what we obtained from the first survey, $X_{\text{CO}} \sim (8 \pm 2) \times 10^{20} \text{ cm}^{-2} (\text{K km s}^{-1})^{-1}$, after taking into account the beam deconvolution but is consistent within the error.

An X_{CO} -factor in the inner Galaxy has been derived by using a correlation between the γ -ray and the CO intensity along the Galactic plane (Bloemen et al. 1986). Bloemen et al. (1986) summarized the value of the X -factors, and the value for the inner Galaxy was derived to be $\sim(1-3) \times 10^{20} \text{ cm}^{-2} (\text{K km s}^{-1})^{-1}$ on

average. The X -factor obtained above is about twice that of the clouds in the inner Galaxy.

Bertoldi & McKee (1992) argue that the gravitational energy, W , of an ellipsoidal cloud is given by $W = -(3/5)(GM^2/R)[\arcsin(e)/e]$, (eq. [A9] of Bertoldi & McKee 1992) where G , M , and R are the gravitational constant, mass, and the size of the clouds, respectively. Here, e is an eccentricity of the cloud, $e = (1 - y^2)^{1/2}$, where y is an axial ratio of the cloud. The current sample of the GMCs are not really spherical, with the mode of the ratio of the major and minor axes being ~ 1.7 and the average being 2.5, as shown in § 3.3 (see also Fig. 8). The shape-dependent factor, $a_2 = (R_m/R)[\arcsin(e)/e]$ (eq. [A8] of Bertoldi & McKee 1992), ranges from 1 to 0.88 for the current sample of the GMCs in the LMC, with $a_2 = 0.99$ for the axis ratio of 2.5. This means that the virial mass of the current sample of the GMCs differs from the derived virial mass with about 15% at most due to the elliptical shape of the clouds. The deviations of the estimated M_{vir} from the true M_{vir} affect the derived X_{CO} -factor linearly. Thus, the current estimate of the X_{CO} -factor can be overestimated

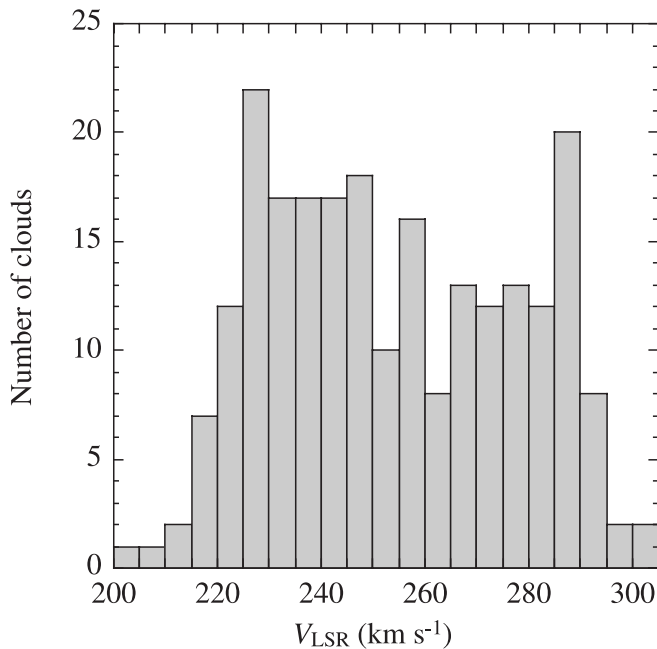


FIG. 7.—Frequency distribution of the V_{LSR} of the clouds.

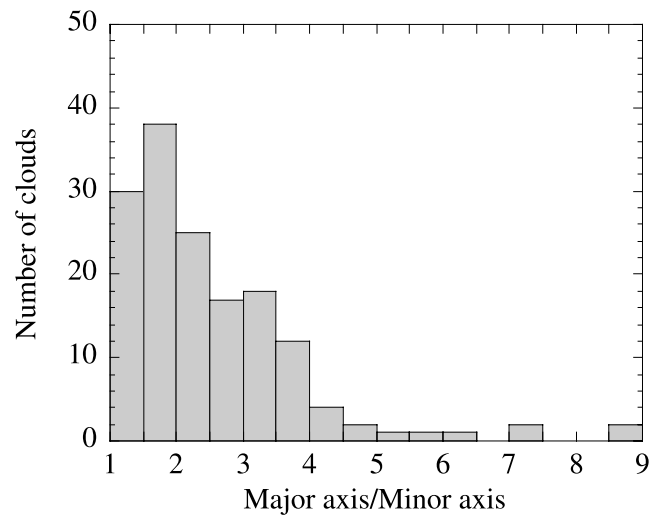


FIG. 8.—Distribution of the ratio of the major and minor axes of the clouds. Both axes are derived by using the FITSTOPROPS program (Rosolowsky & Leroy 2006) and then by deconvolving the NANTEN beam (see § 3).

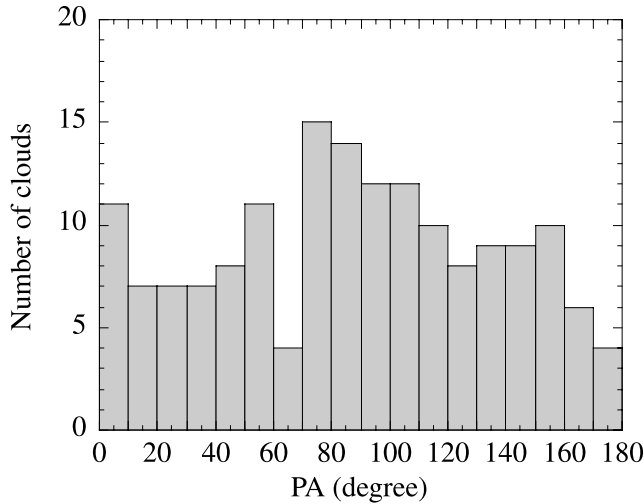


FIG. 9.—P.A. of the clouds. P.A. is taken as 0° toward the north and then increases to the east in the counterclockwise direction.

by at most $\sim 15\%$ due to the deviation of the cloud shape from spherical symmetry.

Rubio et al. (1993) suggested a possible dependence of the X_{CO} -factor on cloud size from their observations toward the clouds in the SMC with SEST. Figure 17 is a plot of the $M_{\text{vir}}/L_{\text{CO}}$

against the cloud size. There is no significant correlation in the LMC clouds; the scatter is as large as an order of magnitude in $M_{\text{vir}}/L_{\text{CO}}$, although the range of the cloud sizes is the same as that of the SMC (Rubio et al. 1993)

It has been claimed that the metallicity is quite uniform in the LMC (e.g., Dufour 1984), while the metallicity of the outer part of a galaxy is suggested to be lower than that of its inner region for our Galaxy and some of the nearby galaxies (e.g., Nakagawa et al. 2005). Figure 18 shows a plot of $M_{\text{vir}}/L_{\text{CO}}$ against the distance from the center of the LMC derived from the H I distribution (Kim et al. 1998). The current result shows no clear correlation of $M_{\text{vir}}/L_{\text{CO}}$ with the distance from the center, suggesting that the X_{CO} -factor does not depend on the distance from the center of the LMC. This is consistent with the idea that the metallicity is quite uniform in the LMC.

4.3. Mass Spectrum

The mass spectrum of the Galactic clouds (^{12}CO or ^{13}CO) is well fitted by a power law with index values of $\alpha \sim 0.5-1.0$ (e.g., Solomon et al. 1987; Solomon & Rivolo 1989; Casoli et al. 1984; Digel et al. 1996; Dobashi et al. 1996), of which the higher values are derived from the lower mass clouds in the outer Galaxy (e.g., Heyer et al. 2001) or from ^{13}CO observations (e.g., Yonekura et al. 1997; Kawamura et al. 1998). The mass distribution of the Galactic clouds and that of the clouds in nearby galaxies have been studied (Blitz et al. 2007 and references therein). Most of the

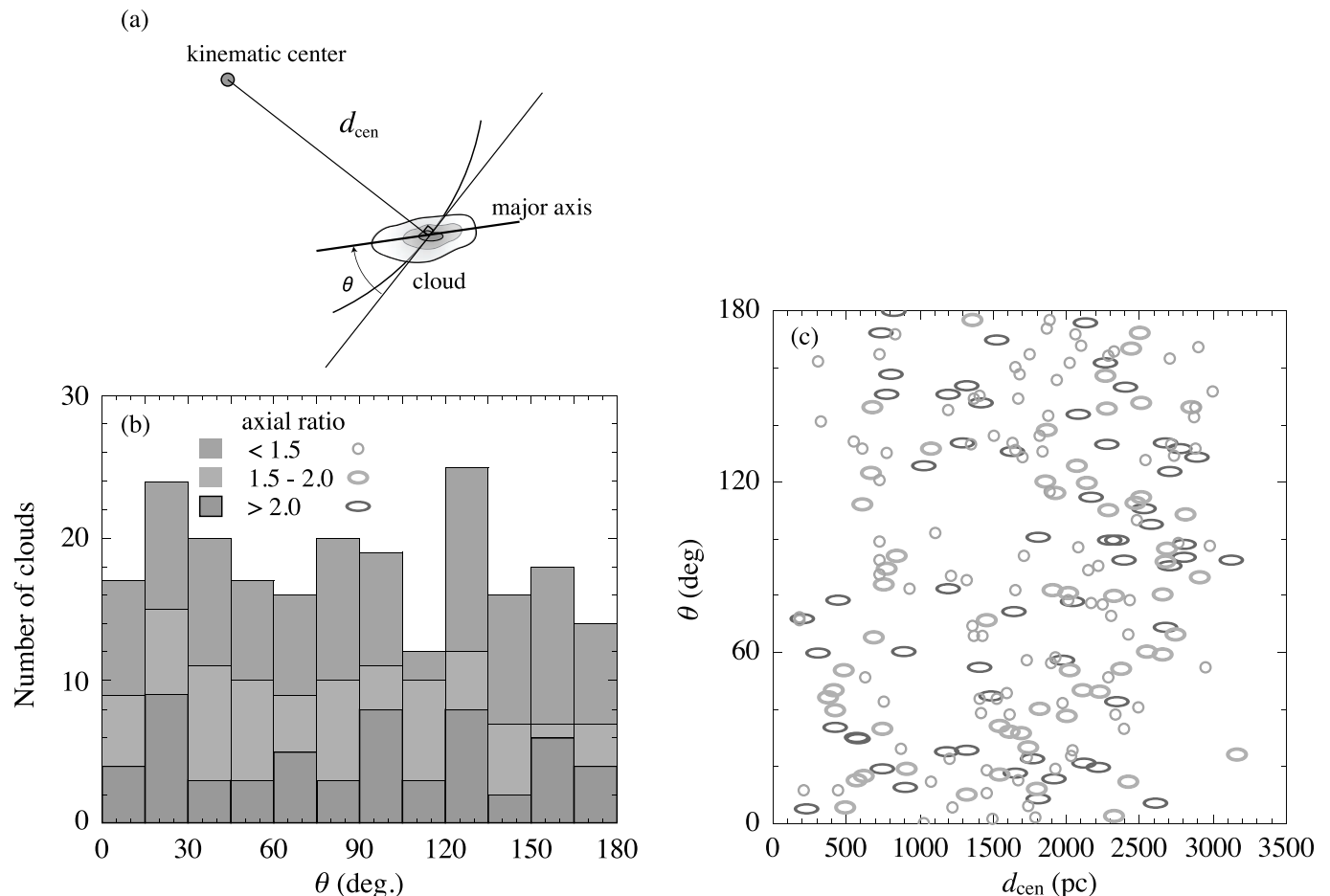


FIG. 10.—(a) Angle, θ , between the major axis of the GMC and the tangent of the circle with a radius of the distance, d_{cen} , from the kinematic center derived from the H I by Kim et al. (1998). (b) Distribution of θ . (c) The angle, θ , with respect to the distance of the GMCs from the center derived from the H I kinematics by Kim et al. (1998). The most elongated ellipses, ellipses, and circles show the GMCs with the ratio of the major and minor axes to be >2.0 , $1.5-2.0$, and <1.5 , respectively. [See the electronic edition of the Supplement for a color version of this figure.]

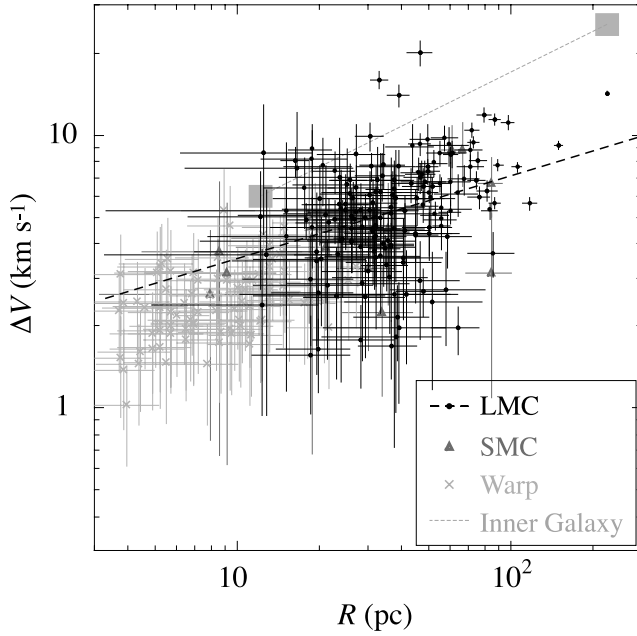


FIG. 11.—Line width–size relation for the GMCs in the LMC (filled circles). Triangles show the clouds in the SMC (Mizuno et al. 2001a) and crosses those in the Warp region (Nakagawa et al. 2005); the clouds in these regions are re-identified by using the algorithm described in Rosolowsky & Leroy (2006) and the same parameters used to identify the clouds in the LMC. The thick dashed line is the best-fitting power law to the GMCs in the LMC, $\Delta V = 1.3R^{0.2}$, with Spearman rank coefficient of 0.3. The relation found for the GMCs in the inner Galaxy from Solomon et al. (1987, thin dotted line) is shown as an example. [See the electronic edition of the Supplement for a color version of this figure.]

galaxies have similar mass distributions, $\alpha \sim 0.7$; an exception is M33, which is steeper than the rest, but the data set has a higher completeness limit (Rosolowsky et al. 2003; Rosolowsky 2005).

A number of numerical simulations have been conducted to obtain a mass spectrum of GMCs in galaxies (e.g., Vázquez-Semadeni

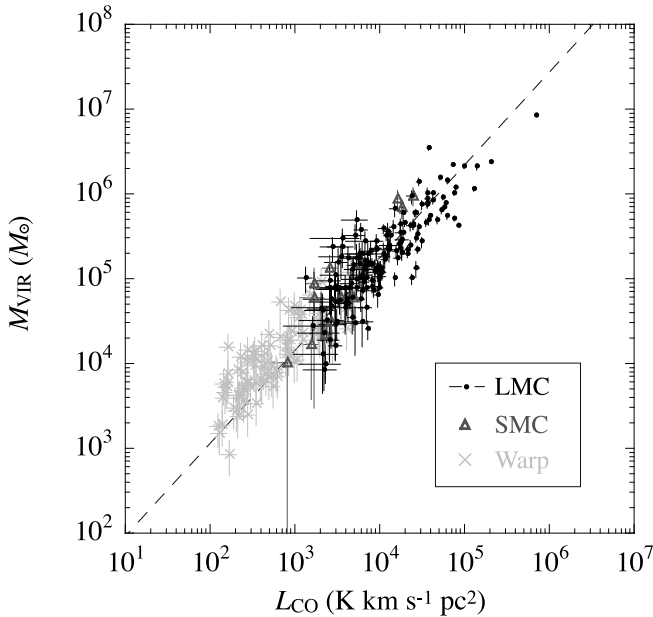


FIG. 12.—Virial mass, M_{vir} of the GMCs as a function of luminosity, L_{CO} (filled circles). The line present a best fit to the data with a slope of 1.1 ± 0.1 . Triangles show the clouds in the SMC (Mizuno et al. 2001a) and crosses those in the Warp region (Nakagawa et al. 2005); the clouds in these regions are re-identified as for the LMC clouds by using the algorithm described by Rosolowsky & Leroy (2006). [See the electronic edition of the Supplement for a color version of this figure.]

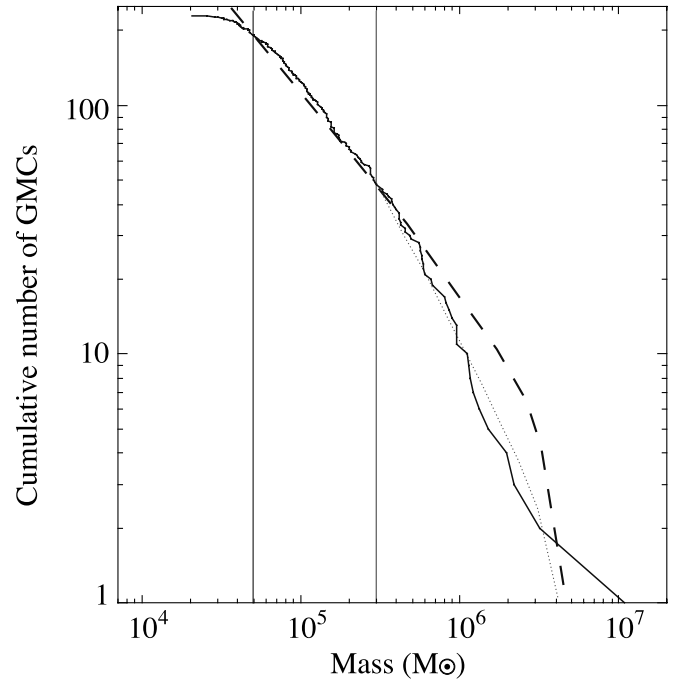


FIG. 13.—Cumulative mass spectra of the 230 GMCs. The best-fitting power law to M_{CO} above the completeness limit $5 \times 10^4 M_{\odot}$ (thick vertical line) is $N_{\text{cloud}}(\geq M_{\text{CO}}) = 6.6 \times 10^5 M_{\text{CO}}^{-0.75 \pm 0.06} - 3.4$ and is indicated by a dashed line. The dotted line indicates the best-fitting power law, $N_{\text{cloud}}(\geq M_{\text{CO}}) = 1.3 \times 10^8 M_{\text{CO}}^{-1.2 \pm 0.2} - 0.72$, obtained by fitting M_{CO} of the 47 clouds with $M_{\text{CO}} \geq 3 \times 10^5 M_{\odot}$ (thin vertical line). [See the electronic edition of the Supplement for a color version of this figure.]

et al. 1997; Wada et al. 2000, and references therein). Wada et al. (2000) carried out a simulation of the H I and CO distributions of an LMC-type galaxy, specifically at the highest spatial resolution (~ 7.8 pc), which incorporated fairly realistic star formation processes and supernova rates. They show that the GMC mass spectrum in an LMC-like galaxy is expected to have a power law with an index value of ~ 0.7 if no star formation is taken into account and that the index becomes steeper, around 1.0, if the dissipation of clouds due to star formation is incorporated. The present mass spectrum appears to be consistent with these values, while those of the non-star-forming models may fit the present result slightly better. According to Wada & Norman (2001), the absence of a massive GMC of $\sim 3 \times 10^6 M_{\odot}$ is due to a well-mixed, turbulent

TABLE 4
SLOPE OF MASS SPECTRUM

Mass Range ^a ($10^4 M_{\odot}$)	α^b	Number of Clouds ^c
>5	0.75 ± 0.06	191
>8	0.88 ± 0.08	146
>10	0.93 ± 0.10	123
>13	0.98 ± 0.11	100
>20	1.0 ± 0.1	67
>30	1.2 ± 0.2	47
>50	1.6 ± 0.3	28

^a Clouds from the 230 GMCs with mass indicated in this column are used to derive a mass spectrum.

^b Index value of the best-fitting power law, $N_{\text{cloud}}(>M) \propto M^{-\alpha}$, to the mass spectrum of the clouds with mass indicated in the first column.

^c Number of the clouds used to fit the power law.

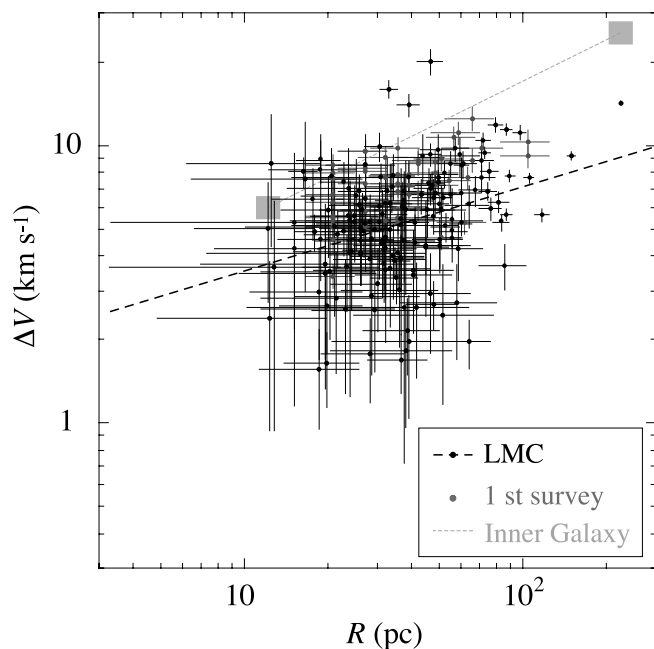


FIG. 14.—Line width–size relation of the Group A GMCs from the current survey (*filled circles*) and 55 “large clouds” from the first survey (*gray filled circles*). The size of a cloud from the first survey was recalculated from the catalog (Mizuno et al. 2001b) by subtracting the NANTEN beam size. The thick dashed line indicates the best-fitting power law of the GMCs from the second LMC survey. The relation found for the GMCs in the inner Galaxy from Solomon et al. (1987, *thin dashed line*) is shown as an example. [See the electronic edition of the Supplement for a color version of this figure.]

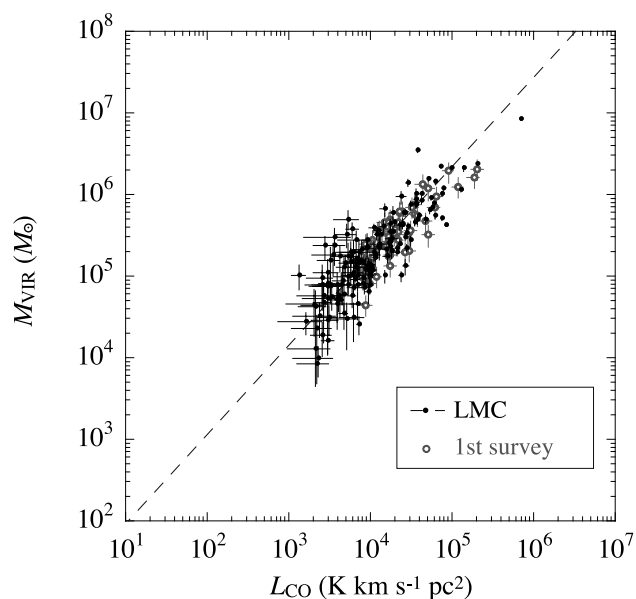


FIG. 15.—Virial mass, M_{vir} , of the 164 GMCs as a function of luminosity, L_{CO} , from the current survey (*filled circles*). The line present a best fit to the data with slope of 1.1 ± 0.1 . Open circles are for the clouds from the first survey (Fukui et al. 1999; Mizuno et al. 2001b). The virial masses of clouds from the first survey were recalculated after subtracting the NANTEN beam size from the sizes of the clouds shown in the catalog of Mizuno et al. (2001b). [See the electronic edition of the Supplement for a color version of this figure.]

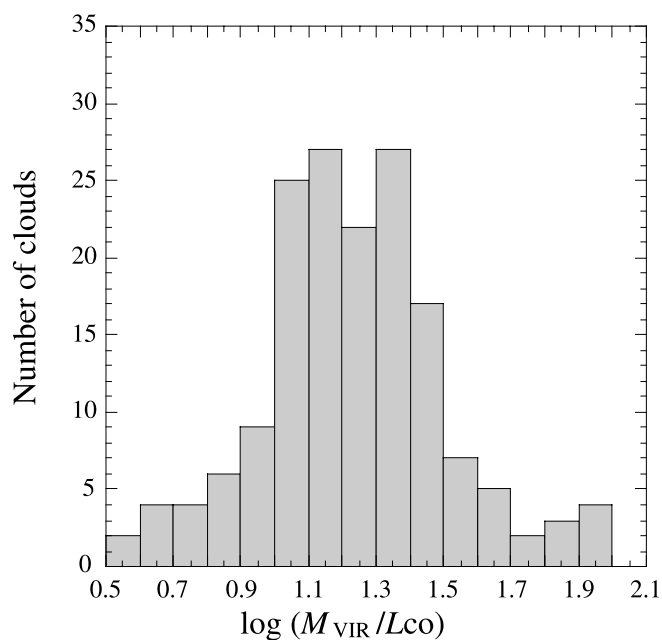


FIG. 16.—Histogram of $\log(M_{\text{vir}}/L_{\text{CO}})$. The mean of $\log(M_{\text{vir}}/L_{\text{CO}})$ is 1.2 ± 0.3 , corresponding to $X_{\text{CO}} = (7 \pm 2) \times 10^{20} \text{ cm}^{-2} (\text{K km s}^{-1})^{-1}$

ISM that tends to form smaller GMCs. The consistency of the mass spectrum among galaxies may suggest that the mechanism of cloud formation and disruption show similar characteristics among galaxies. Nevertheless, the truncation of very massive GMCs may suggest that the disruption of molecular clouds is faster in massive clouds. It may also suggest that cloud formation takes place inhomogeneously; the mass spectra in different regions of the galaxy may have different slopes, and the truncation of the slope might appear when we sum up all the mass spectra within the galaxy. The reason of the truncation is not yet known, but the current results present new information, leading to a better knowledge of cloud formation and disruption.

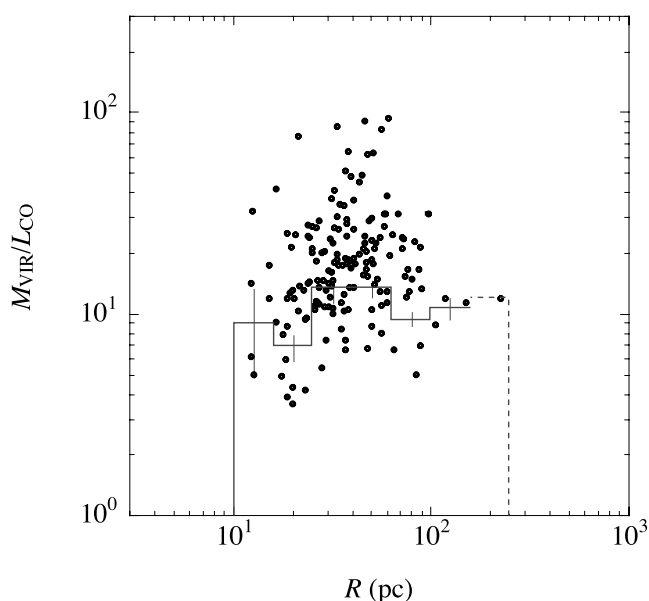


FIG. 17.—Dependence of $M_{\text{vir}}/L_{\text{CO}}$ on the size of the Group A GMCs. The solid line shows the weighted mean of the $M_{\text{vir}}/L_{\text{CO}}$ in each bin of $\log(R)$; the last bin shown by the dashed line includes only one point of $M_{\text{vir}}/L_{\text{CO}}$. [See the electronic edition of the Supplement for a color version of this figure.]

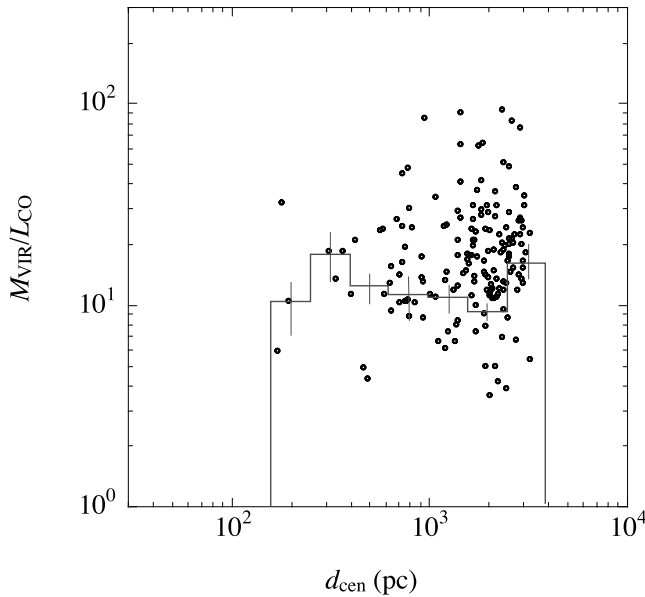


FIG. 18.—Dependence of $M_{\text{vir}}/L_{\text{CO}}$ on the distance of the GMCs from the center of the LMC, $\alpha(\text{J2000.0}) = 5^{\text{h}}17.6^{\text{m}}$, $\delta(\text{J2000.0}) = -69^{\circ}2'$, derived from the H I kinematics (Kim et al. 1998). The solid line shows the weighted mean of $M_{\text{vir}}/L_{\text{CO}}$ in each bin of $\log(d_{\text{cen}})$. [See the electronic edition of the Supplement for a color version of this figure.]

5. SUMMARY

A large-scale ^{12}CO ($J = 1-0$) survey for molecular clouds was made toward the Large Magellanic Cloud (LMC) by NANTEN. An area of $\sim 30 \text{ deg}^2$ was covered, and significant ^{12}CO emission ($\geq 0.07 \text{ K}$) was detected at ~ 1300 out of the 26,900 observed positions. We identified 272 molecular clouds, 230 of which were detected at more than three observing positions. The positions, mean velocities, and velocity dispersions of the 272 clouds, and the extents, position angles, and CO luminosities of the 230 giant molecular clouds (GMCs) are derived. Reliable sizes and virial masses are determined for the well-resolved 164 GMCs (Group A). The main results are summarized as follows.

1. The Group A GMCs have radii ranging from 10 to 220 pc, line widths between 1.6 and 20.2 km s^{-1} , CO luminosities between 1.4×10^3 and $7.1 \times 10^5 \text{ K km s}^{-1} \text{ pc}^2$, masses derived

from CO luminosities from 2×10^4 to $7 \times 10^6 M_{\odot}$, and virial masses from 9×10^3 to $9 \times 10^6 M_{\odot}$. The maximum temperature (T_R^*) of the CO line is as high as $\sim 2 \text{ K}$, which was detected toward the N113 and N159 regions.

2. The line width, ΔV , and the radius, R , of the Group A GMCs appear to satisfy the slope of the power law in the line width–size relation of the clouds in the Galaxy but with an offset in the constant of proportionality.

3. A least-squares fit to the virial mass versus CO luminosity relation shows a power law, $(M_{\text{vir}}/M_{\odot}) = 26[L_{\text{CO}}/(\text{K km s}^{-1} \text{ pc}^2)]^{1.1 \pm 0.3}$, with Spearman rank correlation of 0.8. This good correlation shows that the CO luminosity is a good tracer of the mass of molecular clouds in the LMC.

4. The $I_{\text{CO}}-N(\text{H}_2)$ conversion factor is found to be $X_{\text{CO}} \sim 7 \times 10^{20} \text{ cm}^{-2} (\text{K km s}^{-1})^{-1}$ by assuming virial equilibrium for the Group A GMCs.

5. The mass spectrum of the GMCs with $5 \times 10^4 \leq M_{\text{CO}}/M_{\odot} \leq 10^7$ is well fitted by a power law, $N_{\text{CO}}(> M_{\text{CO}}) \propto (M_{\text{CO}}/M_{\odot})^{-0.75 \pm 0.06}$. This slope is consistent with the previous results obtained from the Galaxy and nearby galaxies. The slope of the mass spectrum becomes steeper if we fit only the massive clouds, e.g., $N_{\text{cloud}}(> M_{\text{CO}}) \propto M_{\text{CO}}^{-1.2 \pm 0.2}$ for $M_{\text{CO}} \geq 3 \times 10^5 M_{\odot}$, which suggests mass truncation.

The NANTEN project is based on a mutual agreement between Nagoya University and the Carnegie Institution of Washington (CIW). We greatly appreciate the hospitality of all the staff members of the Las Campanas Observatory of CIW. We acknowledge Leo Blitz, Erik Rosolowsky, and Adam Leroy for their discussion and providing us with their cloud-identifying program. We are thankful to many Japanese public donors and companies who contributed to the realization of the project. This work is financially supported in part by a Grant-in-Aid for Scientific Research from the Ministry of Education, Culture, Sports, Science and Technology of Japan (15071203) and from the Japan Society for the Promotion of Science (JSPS) (14102003, core-to-core program 17004 and 18684003). T. M. is supported by the JSPS and M. R. by the Chilean Center for Astrophysics, FONDAF 15010003.

REFERENCES

- Bertoldi, F., & McKee, C. 1992, *ApJ*, 395, 140
 Bica, E., Claria, J. J., Dottori, H., Santos, J. F. C., Jr., & Piatti, A. E. 1996, *ApJS*, 102, 57
 Blitz, L., Fukui, Y., Kawamura, A., Leroy, A., Mizuno, N., & Rosolowsky, E. 2007, in *Protostars and Planets V*, ed. B. Reipurth, D. Jewitt, & K. Keil (Tucson: Univ. Arizona Press), 951
 Blitz, L., & Thaddeus, P. 1980, *ApJ*, 241, 676
 Bloemen, J. B. G. M., et al. 1986, *A&A*, 154, 25
 Blum, R. D., et al. 2006, *AJ*, 132, 2034
 Caldwell, D. A., & Kutner, M. L. 1996, *ApJ*, 472, 611
 Casoli, F., Combes, F., & Gerin, M. 1984, *A&A*, 133, 99
 Cohen, R. S., Dame, T. M., Garay, G., Montani, J., Rubio, M., & Thaddeus, P. 1988, *ApJ*, 331, L95
 Crawford, D. F., Jauncey, D. L., & Murdoch, H. S. 1970, *ApJ*, 162, 405
 Dame, T. M., Elmegreen, R. S., Cohen, R. S., & Thaddeus, P. 1986, *ApJ*, 305, 892
 Davies, R. D., Elliott, K. H., & Meaburn, J. 1976, *MmRAS*, 81, 89
 Dickel, J. R., McIntyre, V. J., Gruendl, R. A., & Milne, D. K. 2005, *AJ*, 129, 790
 Digel, S. W., et al. 1996, *ApJ*, 458, 561
 Dobashi, K., Bernard, J. P., & Fukui, Y. 1996, *ApJ*, 466, 282
 Dufour, R. J. 1984, in *IAU Symp. 108, Structure and Evolution of the Magellanic Clouds*, ed. S. van den Bergh & K. S. de Boer (Dordrecht: Reidel), 353
 Filipovic, M. D., Jones, P. A., White, G. L., Haynes, R. F., Meinert, D., Wielebincki, R., & Klein, U. 1996, *A&AS*, 120, 77
 Fukui, Y. 2002, in *ASP Conf. Ser. 285, Modes of Star Formation and the Origin of Field Populations*, ed. E. K. Grebel & W. Brandner (San Francisco: ASP), 24
 ———. 2005, in *IAU Symp. 227, Massive Star Birth: A Crossroads of Astrophysics*, ed. R. Cesaroni et al. (Cambridge: Cambridge Univ. Press), 328
 ———. 2007, in *IAU Symp. 237, Triggered Star Formation in a Turbulent ISM*, ed. B. Elmegreen & J. Palous (Cambridge: Cambridge Univ. Press), 31
 Fukui, Y., Mizuno, N., Yamaguchi, R., Mizuno, A., & Onishi, T. 2001, *PASJ*, 53, L41
 Fukui, Y., & Sakakibara, O. 1992, *Mitsubishi electronic ADVANCE*, 60, 11
 Fukui, Y., et al. 1999, *PASJ*, 51, 745
 Haynes, R. F., et al. 1991, *A&A*, 252, 475
 Henize, K. G. 1956, *ApJS*, 2, 315
 Heyer, M. H., Carpenter, J. M., & Snell, R. L. 2001, *ApJ*, 551, 852
 Hibi, Y., Shibai, H., Kawada, M., Ootsubo, T., & Hirashita, H. 2006, *PASJ*, 58, 509
 Hodge, P. 1988, *PASP*, 100, 1051
 Hughes, A., Wong, T., Ekers, R., Staveley-Smith, L., Filipovic, M., Maddison, S., Fukui, Y., & Mizuno, N. 2006, *MNRAS*, 370, 363
 Israel, F. P., de Graauw, Th., van de Stadt, H., & de Vries, C. P. 1986, *ApJ*, 303, 186

- Israel, F. P., et al. 2003, *A&A*, 406, 817
- Ita, Y., et al. 2004, *MNRAS*, 347, 720
- Johansson, L. E. B., Olofsson, H., Hjalmarson, Å., Gredel, R., & Black, J. H. 1994, *A&A*, 291, 89
- Johansson, L. E. B., et al. 1998, *A&A*, 331, 857
- Kato, D. et al. 2007, *PASJ*, 59, 615
- Kawamura, A., Onishi, T., Yonekura, Y., Dobashi, K., Mizuno, A., Ogawa, H., & Fukui, Y. 1998, *ApJS*, 117, 387
- Kawamura, A., Minamidani, T., Mizuno, Y., Onishi, T., Mizuno, N., Mizuno, A., & Fukui, Y. 2007, in *IAU Symp. 237, Triggered Star Formation in a Turbulent ISM*, ed. B. G. Elmgreen & J. Palous (Cambridge: Cambridge Univ. Press), 101
- . 2008, *ApJS*, submitted (Paper II)
- Kennicutt, R. C., Jr., & Hodge, P. W. 1986, *ApJ*, 306, 130
- Kim, S., Dopita, M. A., Staveley-Smith, L., & Bessel, M. S. 1999, *AJ*, 118, 2797
- Kim, S., Staveley-Smith, L., Dopita, M. A., Freeman, K. C., Sault, R. J., Kesteven, M. J., & McConnell, D. 1998, *ApJ*, 503, 674
- Koornneef, J. 1982, *A&A*, 107, 247
- Kutner, M., & Ulich, B. L. 1981, *ApJ*, 250, 341
- Kutner, M. L., et al. 1997, *A&AS*, 122, 255
- Larson, R. B. 1981, *MNRAS*, 194, 809
- Lucke, P. B., & Hodge, P. W. 1970, *AJ*, 75, 171
- Luks, Th., & Rohlf, K. 1992, *A&A*, 263, 41
- McGee, R. X., & Milton, J. A. 1966, *Australian J. Phys.*, 19, 343
- Meaburn, J. 1980, *MNRAS*, 192, 365
- Meixner, M., et al. 2006, *AJ*, 132, 2268
- Mizuno, N., Rubio, M., Mizuno, A., Yamaguchi, R., Onishi, T., & Fukui, Y. 2001a, *PASJ*, 53, L45
- Mizuno, N., et al. 2001b, *PASJ*, 53, 971
- Nakagawa, M., Onishi, T., Mizuno, A., & Fukui, Y. 2005, *PASJ*, 57, 917
- Ogawa, H., Mizuno, A., Hoko, H., Ishikawa, H., & Fukui, Y. 1990, *Int. J. Infrared and Millimeter Waves*, 11, 717
- Ohta, K., Tomita, A., Saito, M., Sasaki, M., & Nakai, N. 1993, *PASJ*, 45, L21
- Rohlf, K., Kreitschmann, J., & Feitzinger, J. V. 1984, in *IAU Symp. 108, Structure and Evolution of the Magellanic Clouds*, ed. S. van den Bergh & K. S. D. Boer (Dordrecht: Reidel), 395
- Rolleston, W. R. J., Trundle, C., & Dufton, P. L. 2002, *A&A*, 396, 53
- Rosolowsky, E. 2005, *PASP*, 117, 1403
- Rosolowsky, E., Engargiola, G., Plambeck, R., & Blitz, L. 2003, *ApJ*, 599, 258
- Rosolowsky, E., & Leroy, A. 2006, *PASP*, 118, 590
- Rubio, M., Lequeux, J., & Boulanger, F. 1993, *A&A*, 271, 9
- Sakon, I., et al. 2006, *ApJ*, 651, 174
- Scoville, N. Z., Yun, M. S., Sanders, D. B., Clemens, D. P., & Waller, W. H. 1987, *ApJS*, 63, 821
- Snowden, S. L., & Petre, R. 1994, *ApJ*, 436, L123
- Solomon, P. M., & Rivolo, A. R. 1989, *ApJ*, 339, 919
- Solomon, P. M., Rivolo, A. R., Barrett, J., & Yahil, A. 1987, *ApJ*, 319, 730
- Vázquez-Semadeni, E., Ballesteros-Paredes, J., & Rodríguez, L. F. 1997, *ApJ*, 474, 292
- Wada, K., & Norman, C. A. 2001, *ApJ*, 547, 172
- Wada, K., Spaans, M., & Kim, S. 2000, *ApJ*, 540, 797
- Wilson, C. D., & Scoville, N. 1990, *ApJ*, 363, 435
- Wong, T., & Blitz, L. 2000, *ApJ*, 540, 771
- . 2002, *ApJ*, 569, 157
- Yamaguchi, R., Mizuno, N., Onishi, T., Mizuno, A., & Fukui, Y. 2001a, *ApJ*, 553, 185L
- . 2001b, *PASJ*, 53, 959
- Yamaguchi, R., et al. 2001c, *PASJ*, 53, 985
- Yonekura, Y., Dobashi, K., Mizuno, A., Ogawa, H., & Fukui, Y. 1997, *ApJS*, 110, 21
- Young, J. S., & Scoville, N. Z. 1991, *ARA&A*, 29, 581
- Zaritsky, D., Harris, J., Thompson, I. B., & Grebel, E. K. 2004, *AJ*, 128, 1606